UCRL-90602
PREPRINT

Direct Implicit Plasma Simulation

A. Bruce Langdon,
Lawrence Livermore National Laboratory

D. C. Barnes,
Institute for Fusion Studies

A chapter in the volume
"Multiple Time Scales"
in the series
Computational Techniques,
Academic Press, 1984

March 27, 1984

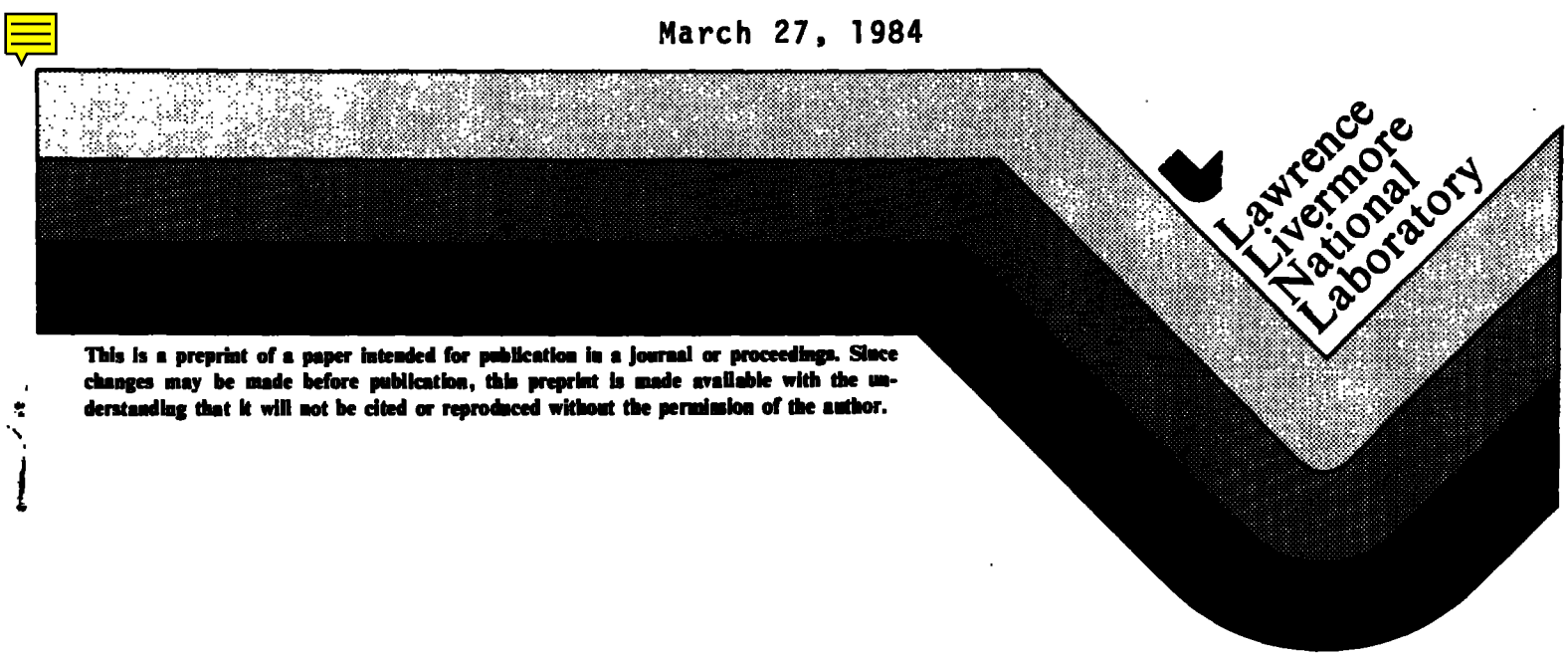

DISCLAIMER

UCRL-90602, March 1984

DIRECT IMPLICIT PLASMA SIMULATION

A. Bruce Langdon

Lawrence Livermore Laboratory
Physics Department
University of California
Livermore, California, 94550

D. C. Barnes

Institute for Fusion Studies
The University of Texas at Austin
Austin, Texas 78712

A chapter in the volume
"Multiple Time Scales"
in the series
Computational Techniques,
Academic Press, 1984.

CONTENTS

	Page
I. Introduction	1
I.A. Characteristic Time Scales in Weakly-Collisional Plasma	2
I.B. PIC Electrostatic Force Calculation	2
I.C. Explicit Time Differencing of Particle Motion	4
I.D. Implicit Time Differencing of the Particle Equations	5
II. Direct Method With Electrostatic Fields	6
II.A. Solution of the Implicit Equations	6
1. Outline of the "direct method"	7
2. A one-dimensional realization	8
3. Simplified Differencing	9
4. General electrostatic case	10
5. Iterative Solution of Corrector Equation in Two Dimensions with Magnetic Field	13
6. Comparison to the "Moment" Method	14
II.B. Representative results	15
1. Free expansion of a plasma slab	15
2. Ion-acoustic fluctuations of a nonequilibrium plasma	16
3. Gravitational interchange instability of a magnetized plasma	17
II.C. Properties of Implicit Particle Codes	18
1. Remaining limitations on time step	18
Doppler frequency limit	18
Limits due to field and density gradients	19
2. Momentum Conservation	20
3. Energy Conservation and Artificial Cooling	22
4. Effects of imperfect field solution on linear stability and dispersion	25
Non-strict differencing and inconsistent filtering	25
Nonlocal susceptibility	26
III. Gyro Averaged Particle Simulation (GAPS)	27
III.A Individual Particle Motion	27
III.B The Direct Method for Electrostatic GAPS	30
IV. Electromagnetic Direct Implicit Method	32
IV.A Darwin, or Magnetoinductive, Fields	33
IV.B Implicit Electromagnetic Fields	34
IV.C The Direct Method for Implicit Particles and Fields	36
IV.D Comparison of Darwin and Implicit Codes	39
V. Concluding Remarks	40
ACKNOWLEDGMENTS	40
REFERENCES	41
FIGURES	46

I. INTRODUCTION

Characteristic time scales for collective phenomena in plasmas encompass many orders of magnitude. Where kinetic effects are crucial, i.e. fluid descriptions are inadequate, computer simulation methods have been applied very successfully to studies of the nonlinear evolution of plasma phenomena on the faster time scales. For both applications and basic studies, there is increasing interest in extending simulation techniques to kinetic phenomena on much longer time scales.

One approach to modelling long time-scale behavior in such systems is to alter the governing equations to eliminate uninteresting high frequency modes. Examples include the electrostatic and Darwin field approximations in plasma simulation, and incompressible hydrodynamics. Other approaches, described here and in other chapters in this volume, are subcycling, orbit-averaging and implicit time integration.

The most adaptable and reliable tools for study of complex kinetic plasma behavior are the "particle-in-cell" (PIC) codes, in which the plasma evolution is modelled by 10^3–10^7 simulation "particles", each representing a large number of plasma particles, and moving according to the classical Newton-Lorentz equations of motion in fields governed by Maxwell's equations. In plasmas, many instability, dissipation and nonlinear saturation mechanisms are kinetic in nature. As particle codes have been very successful in studying such phenomena, improving their efficiency for long-time-scale simulation is of great value.

This Chapter describes a method for implementing implicit time differencing in PIC plasma codes, in which the equations for the time-advanced quantities are constructed directly from the particle equations of motion by linearization, rather than by introducing fluid (velocity moment) equations. This "direct" method is outlined in Section II.A.1; a simple but practical implementation is in Section II.A.3.

The divisions of this chapter are as follows: The remainder of this Section defines the explicit electrostatic PIC algorithm, introducing the notation to be used throughout this Chapter, and outlines the properties of explicit differencing and the implicit scheme we use. Section II presents the direct method as applied to the electrostatic field case, some results, and discusses remaining limitations on time step, conservation properties, and linear stability theory. For strongly magnetized plasma, the gyro-averaged algorithm in Section III removes the unwanted large cyclotron frequency. In Section IV the direct method is generalized to include the full electromagnetic field.

I.A. Characteristic Time Scales in Weakly-Collisional Plasma

The highest frequencies are associated with the small mass of electrons and the high speed of light. The Langmuir frequency, ω_{pe}, also called simply the plasma frequency, characterizes charge-separation oscillations. Others include the cyclotron frequency, ω_{ce}, and the transit time for electrons or light to cross a characteristic distance.

In contrast, long time scales can be set by ion inertia, electromagnetic effects, and large spatial scale lengths. The ratios of electron to ion plasma and cyclotron frequencies, and of hydrodynamic to electron transit times, are determined by the small number Zm_e/m_i, where Z is the ionic charge state. Where the dominant forces are from magnetic fields due to currents in the plasma itself, the frequencies are reduced relative to ω_{pe} by at least the ratio c/v_e, where c and v_e are light and electron speeds.

I.B. PIC Electrostatic Force Calculation

The plasma simulation models treated here use a spatial grid to mediate the particle interactions. Originally developed at Stanford, this approach is used in some form in almost all modern plasma work. Rather than summing interactions over particle pairs, a charge density is formed from the particle positions onto a spatial grid. Using partial difference equations on this grid, an electric field is found. Then the particles are individually advanced in time using classical equations of motion with the acceleration found by interpolation from the electric field on the grid. This method is not only faster than summing over particle interactions, it avoids very large accelerations of closely spaced particles, which create complications irrelevant to the simulation of collective effects in weakly collisional plasma.

In the description and analysis of these algorithms, it is helpful to consider the charge of the particle to be a diffuse "cloud", with $qS(x)$ the charge density of a particle whose center is at the origin. The charge density of a plasma with particle number density $n(x,t)$ is

$$\rho_c(x,t) = S(x)*qn(x,t) = \int dx'\ S(x-x')\ qn(x',t) \qquad (I.1)$$

where the asterisk denotes convolution. This charge density is sampled at the lattice points of a regular grid in space. To avoid clutter we will temporarily restrict the discussion to one dimension. The charge density associated with grid point j is taken to be $\rho_j(t) = \rho_c(X_j,t)$, where $X_j \equiv j\Delta x$, and Δx is the grid spacing. In practice, the contribution of each simulation particle is added to ρ_j

$$\rho_j = \sum_i q_i S(X_j - x_i) \qquad (I.2)$$

where i is the particle index, q_i is the charge, and S is the particle-grid interpolation spline.

The form of the weighting function S(x) is designed to provide good numerical properties. As developed originally at Stanford, these models used "nearest-grid-point" weighting between particle and grid quantities (Hockney, 1965; Burger *et al*, 1965; Yu *et al*, 1965; Boris and Roberts, 1969). Most present work is done with linear weighting (Birdsall and Fuss, 1969; Morse and Nielson, 1969). In one dimension, S is the linear spline, a tent-shape extending over two cells and zero elsewhere.

From ρ a potential and electric field are derived on the same mesh. These satisfy relations such as

$$E_j = - \frac{\phi_{j+1} - \phi_{j-1}}{2\Delta x} \equiv - \nabla_j \phi \qquad (I.3)$$

$$\frac{\phi_{j+1} - 2\phi_j + \phi_{j-1}}{\Delta x^2} = - \rho_j \qquad (I.4)$$

in rationalized cgs units (Panofsky and Phillips, 1962; Jackson, 1962).

Additional smoothing is often applied to ρ_j or ϕ_j. Consider this to be a convolution with a function $\hat{S}$.

The particle force field is obtained by an interpolation of the form

$$F_i = q_i \Delta x \sum_j E_j \, S(X_j - x_i) \qquad (I.5)$$

where the sum is over grid points j and S is the same function used in (I.2).

In three dimensions the locations of grid points are given by

$$X_j = (j_x \Delta x, \, j_y \Delta y, \, j_z \Delta z) = \mathbf{j} \cdot \Delta \mathbf{x} \qquad (I.6)$$

where j is a vector with integer components and $\Delta \mathbf{x}$ is a tensor. In the simplest case of a cubic mesh with spacing Δx, X_j is just $j\Delta x$. In (I.5) Δx is replaced by $|\Delta \mathbf{x}| = \det \Delta \mathbf{x}$, the volume of one grid cell.

We will maintain a convention in which n and F refer to particle

quantities defined on a spatial continuum, while ρ, ϕ, and **E** are defined on the spatial grid.

I.C. Explicit Time Differencing of Particle Equations of Motion

For the integration of the particle equations of motion numerical time differencing algorithms of the elegant type discussed by Buneman (1967) are almost universally used.

$$\frac{x_{n+1} - x_n}{\Delta t} = v_{n+\frac{1}{2}}; \qquad \frac{v_{n+\frac{1}{2}} - v_{n-\frac{1}{2}}}{\Delta t} = a_n + \frac{v_{n+\frac{1}{2}} + v_{n-\frac{1}{2}}}{2} \times \frac{qB_n}{mc} \qquad (I.7ab)$$

$$\text{where } a_n = \frac{q}{m} E_n(x_n), \qquad (I.7c)$$

and subscript n denotes time level $t_n = n\Delta t$. This is usually called the centered leapfrog scheme.

Equations (I.2, I.3, I.4, I.5 and I.7ab) outline the time cycle of an explicit PIC simulation.

In the simplest, unmagnetized case, longitudinal oscillations in a uniform cold plasma consist simply of harmonic oscillations. The properties of the leapfrog scheme are illustrated by considering a single particle with a linear restoring force, $a_n = -\omega_0^2 x_n$, with no magnetic field term. Setting $x_n = Xz^n = X \exp(-i\omega n\Delta t)$, where $z \equiv \exp(-i\omega\Delta t)$ is the (complex) change in an amplitude per time step, we find

$$(\omega_0\Delta t)^2 = -(z-1)^2/z \qquad (I.8)$$

$$= 4\sin^2(\omega\Delta t/2)$$

For $\omega_0\Delta t < 2$, the roots z lie on the unit circle, i.e. ω is real: the oscillations are neither growing nor damped. This property is valuable in plasmas, where oscillatory behavior is ubiquitous and the distinction of stable and growing oscillations is crucial to many studies.

For $\omega_0\Delta t > 2$, one root z lies *outside* the unit circle (Im $\omega > 0$); this numerical instability arises for *any explicit* scheme for $\omega_0\Delta t$ above some threshold of order unity (Cohen *et al*, 1982b). Instability can be avoided through the use of implicit time integration, at the expense of increased complexity.

I.D. Implicit Time Differencing of the Particle Equations of Motion

The first major issue is the choice of finite-differenced equations of motion for the particles which have the necessary stability at large time-step and are accurate for the low frequency phenomena to be simulated. We choose not to consider backward-biased schemes with relative errors of order Δt. It is not expensive to achieve relative error of order Δt^2, with error Δt^3 in Im ω, the growth/decay rate.

Several suitable schemes for time-differencing the particles have been analyzed and applied (Cohen *et al*, 1982b). Here, we will discuss only the "D_1" scheme, also called the $\bar{1}$ scheme (Barnes *et al*, 1983b), which can be written

$$\frac{x_{n+1} - x_n}{\Delta t} = v_{n+\frac{1}{2}}; \qquad \frac{v_{n+\frac{1}{2}} - v_{n-\frac{1}{2}}}{\Delta t} = \bar{a}_n + \frac{v_{n+\frac{1}{2}} + v_{n-\frac{1}{2}}}{2} \times \frac{qB_n}{mc} \tag{I.9ab}$$

$$\text{where } \bar{a}_n = \tfrac{1}{2}[\bar{a}_{n-1} + \tfrac{q}{m}E_{n+1}(x_{n+1})]. \tag{I.10}$$

Or, if the recursive filter is applied to the fields rather than to the particles (Barnes *et al*, 1983b), we write

$$\bar{a}_n = \frac{q}{m}\bar{E}_n(x_n) = \tfrac{1}{2}\frac{q}{m}\left[\bar{E}_{n-1}(x_n) + E_{n+1}(x_n)\right], \tag{I.11}$$

$$\text{where } \bar{E}_n = \tfrac{1}{2}[\bar{E}_{n-1} + E_{n+1}]. \tag{I.12}$$

This choice saves storage of one vector quantity per particle, relative to (I.10). In fact, the particle mover coding is exactly the same as for the explicit leap-frog method (I.7)! The only difference is that the electric acceleration is from $\bar{E}_n$ instead of E_n. Note that E_{n+1} is evaluated at *different* positions in (I.10) and (I.11). This creates side effects which we discuss in sections II.A, II.C.2 and II.C.4.

To check the accuracy of this scheme, we can derive and solve a dispersion relation for harmonic oscillations, analogous to (I.8):

$$(\omega_0\Delta t)^2 + (2/z - 1/z^2)(z - 1)^2/z = 0 \tag{I.13}$$

For $\omega_0\Delta t \lesssim 1$, we find (Cohen *et al*, 1982b)

$$\pm \mathrm{Re}\ \omega/\omega_0 = 1 - (11/24)(\omega_0\Delta t)^2 + \ldots, \quad \mathrm{Im}\ \omega/\omega_0 = -(\omega_0\Delta t)^3/2 + \ldots,$$

and an extraneous damped mode with $|z| \to \frac{1}{2}$. For $\omega_0\Delta t >> 1$, the modes are heavily damped, $|z| \to (\omega_0\Delta t)^{-2/3}$.

Equation (I.9b) can be solved exactly for $v_{n+\frac{1}{2}}$ by adding $\frac{1}{2}\bar{a}_n\Delta t$ to $v_{n-\frac{1}{2}}$, doing a rotation, and again adding $\frac{1}{2}\bar{a}_n\Delta t$. The result is

$$v_{n+\frac{1}{2}} = \tfrac{1}{2}\bar{a}_n\Delta t + R\cdot[v_{n-\frac{1}{2}} + \tfrac{1}{2}\bar{a}_n\Delta t] \qquad (I.14)$$

where the operator R effects a rotation through angle $-2\tan^{-1}(\Omega\Delta t/2)$ (where $\Omega \equiv qB_n/mc$), and can be written

$$(1+\theta^2)R = (1-\theta^2)I + 2\theta\theta - 2\theta\times I, \qquad (I.15)$$

where $\theta = \Omega\Delta t/2$ and I is the unit tensor. For small $\Omega\Delta t$, $R \cong I - \Omega\Delta t\times I$. For large $\Omega\Delta t$, $R \cong -I + 2\Omega^{-2}\Omega\Omega - (4/\Omega^2\Delta t)\Omega\times I$.

The optimum design of these time-difference equations is the first, but simpler, issue in practical implementation of large time-step methods.

With explicit differencing, the time-cycle is split between advancing particles and fields; these calculations alternate and proceed independently. A price we pay for implicit differencing is that time-cycle splitting is more complicated. An implicit code must solve the coupled set of equations (I.2) through (I.5), with (I.9-I.10) or (I.11-I.12). This is the second issue in implementation.

II. DIRECT METHOD WITH ELECTROSTATIC FIELDS

In all implicit schemes the future positions x_{n+1} depend on the accelerations a_{n+1} due to the electric field E_{n+1}. But this field is not yet known, as it depends on the density ρ_{n+1} of particle positions $\{x_{n+1}\}$. The solution of this large system of nonlinear, coupled particle and field equations is the other major implementation issue.

II.A. Solution of the Implicit Equations

In the first method implemented for this solution, the fields at the new time level are predicted by solving coupled field and fluid equations, in which the kinetic stress tensor is approximately evaluated from particle velocities known at the earlier time. After the fields are known, the particles are advanced to the new time-level, and, if desired, an improved stress tensor is calculated and the process iterated. This approach has been described in detail by Denavit (1981), and Mason (1981a).

It is also practical to predict the future electric field E_{n+1} quite directly by means of a linearization of the particle–field equations. One form of this method, its implementation, and some examples verifying its performance, have been outlined by Friedman *et al* (1981). Another form is described by Barnes *et al* (1983b); compare (I.10) and (I.11–I.12), and see Section II.C.4. Langdon *et al* (1983) explore the algorithm with great generality, and consider many important details, such as spatial differencing and filtering, and iterative solution of the implicit equations.

1. Outline of the "direct method"

The essence of the "direct" method is that we work *directly* with the particle equations of motion and the particle/field coupling equations. These are linearized about an estimate (extrapolation) for their values at the new time level n+1. The future values of $\{x,v\}$ are divided into two parts:

- increments $\{\delta x,\delta v\}$ which depend on the (unknown) fields at the future time level n+1, and
- extrapolations $\{x_{n+1}^{(0)},v_{n+\frac{1}{2}}^{(0)}\}$ which incorporate *all* other contributions to the equation of motion.

The charge density $\rho_{n+1}^{(0)}$ corresponding to positions $\{x_{n+1}^{(0)}\}$ is collected, as are the coefficients in an expression for the difference $\delta\rho(\{\delta E\}) = \rho_{n+1} - \rho_{n+1}^{(0)}$ between the densities obtained after integration with $E_{n+1}^{(0)}$ and with the corrected field $E_{n+1} = \delta E + E_{n+1}^{(0)}$. These comprise the source term in Gauss' law

$$\nabla\cdot E_{n+1} = \delta\rho(\{\delta E\}) + \rho_{n+1}^{(0)} \qquad (II.1)$$

This becomes a linear elliptic equation, for $\delta\phi$ or ϕ_{n+1}, with non-constant coefficients.

The care with which we express the increment $\{\delta\rho\}$ is a compromise between complexity and strong convergence (Langdon *et al*, 1983; Barnes *et al*, 1983b). If necessary, $\delta\rho$ may be evaluated rigorously as derivatives of equation (I.2) ("strict differencing"; (Langdon *et al*, 1983, section 4), or as simplified difference representations (Langdon *et al*, 1983, Section 3.4; Barnes *et al*, 1983b) of (II.10) for each species. In the following subsections, we consider these two cases in one dimension, generalize to higher dimensions and to include a magnetic field, and briefly discuss an iterative solution of the field equation in two dimensions.

2. A one-dimensional realization

The direct implicit method is illustrated in the following one-dimensional unmagnetized electrostatic example. The position x_{n+1} of a particle at time level t_{n+1}, as given by an implicit time integration scheme, can be written as

$$x_{n+1} = \beta\Delta t^2 a_{n+1} + \tilde{x}_{n+1}, \tag{II.2}$$

where $\beta > 0$ is a parameter controlling implicitness and is $\frac{1}{2}$ for the D_1 scheme; $\tilde{x}_{n+1}$, the position obtained from the equation of motion with the acceleration a_{n+1} omitted, is known in terms of positions, velocities and accelerations at times t_n and earlier. Eliminating $v_{n+\frac{1}{2}}$ between (I.9)-(I.10), we find

$$\tilde{x}_{n+1} = x_n + v_{n-\frac{1}{2}}\Delta t + \tfrac{1}{2}\bar{a}_{n-1}\Delta t^2 \tag{II.3}$$

In its most obvious form, which we adopt for this example, the direct implicit algorithm is derived by linearization of the particle positions relative to $\tilde{x}_{n+1}$, that is, $E^{(0)}_{n+1} = 0$ and therefore $x^{(0)}_{n+1} = \tilde{x}_{n+1}$.

At the grid point located at $X_j \equiv j\Delta x$, the charge density $\tilde{\rho}_{j,n+1}$ is formed as in (I.2) by adding the contribution of the simulation particles at positions $\{\tilde{x}_{i,n+1}\}$.

$$\tilde{\rho}_{j,n+1} = \sum_i q_i S(X_j - \tilde{x}_{i,n+1}) \tag{II.4}$$

If we expand S in (I.2) with respect to position, then

$$\delta\rho_{j,n+1} = -\sum_i q_i\, \delta x_i\, S'(X_j - \tilde{x}_{i,n+1}) \tag{II.5}$$

with $\delta x_i = x_{i,n+1} - \tilde{x}_{i,n+1}$ and $S'(X) = dS/dX$. In terms of E_{n+1}, the particle acceleration is obtained from (I.5) evaluated at $\tilde{x}_{n+1}$.

$$m_i a_{i,n+1} = q_i\Delta x \sum_j E_{j,n+1}\, S(X_j - \tilde{x}_{i,n+1}) \tag{II.6}$$

From the particle equation of motion in the form (II.2),

$$\delta x_i = \beta\Delta t^2\, a_{i,n+1} \tag{II.7}$$

$$= \beta\Delta t^2 (q_i/m_i)\Delta x \sum_j S(X_j - \tilde{x}_{i,n+1}) E_{j,n+1}$$

The densities $\tilde{\rho}_{n+1}$ and $\delta\rho_{n+1}$ are inserted into the field equations (I.3–I.4). With summation over species understood, Poisson's equation in rationalized c.g.s. units becomes

$$-\tilde{\rho}_{j,n+1} = \frac{\phi_{j+1,n+1} - 2\phi_{j,n+1} + \phi_{j-1,n+1}}{\Delta x^2} \tag{II.8}$$

$$+ \Delta x \sum_{i,k} (\beta q_i^2 \Delta t^2/m_i)\, S'(X_j - \tilde{x}_{i,n+1}) S(X_k - \tilde{x}_{i,n+1}) \frac{\phi_{k+1,n+1} - \phi_{k-1,n+1}}{2\Delta x}$$

For linear splines, $\Delta x^2 S'(x) = \pm 1$ or 0, there is no contribution for $|j-k| > 1$, and therefore the field equation is penta-diagonal. After solution of (II.8), E is formed using (I.3), then the particles can be brought serially to their new positions using (II.2) or its equivalent.

The derivation of (II.8) respects the actual field interpolation and charge weighting used with the particles; because of this and its linear stability properties, we call this a "strict" implementation of the direct method. Further discussion is found in Friedman *et al* (1981), Sec. 2 of Langdon *et al* (1983), Cohen *et al* (1984), and Section II.C.2 of this Chapter.

3. Simplified Differencing

It is convenient to implement a simpler field equation than (II.8), while retaining benefits of the direct method. Writing (II.5) as

$$\delta\rho = -\left[\nabla\cdot\sum q\, \delta x\, S(x - \tilde{x}_{n+1})\right]_{x=X_j} \tag{II.9}$$

we see that (II.5) and (II.8) are finite element representations of

$$\delta\rho = -\nabla\cdot[\tilde{\rho}\delta x], \tag{II.10}$$

and the elliptic partial difference equation

$$-\tilde{\rho} = \nabla\cdot[1 + \chi(x)]\nabla\phi \tag{II.11}$$

where $\chi(x) = \beta\tilde{\rho}(x)(q/m)\Delta t^2$ summed over species, i.e. $\chi = \beta(\omega_p\Delta t)^2$. Because of the similarity of (II.11) to the field equation in dielectric media, we call χ the implicit susceptibility. Where $\omega_p\Delta t$ is large, the regime we wish to access, note that $\chi >> 1$ is dominant in the right-hand-side of (II.11).

With the extrapolated charge density $\tilde{\rho}_{j,n+1}$ and a reasonable

finite-difference representation of the linearized implicit contribution $\delta\rho = -\partial(\chi E)/\partial x$, the field equation in one dimension is

$$\tilde{\rho}_{j,n+1} = \left[(1+\chi_{j+\frac{1}{2}})E_{j+\frac{1}{2},n+1} - (1+\chi_{j-\frac{1}{2}})E_{j-\frac{1}{2},n+1}\right]/\Delta x, \qquad (II.12)$$

Two representation of $\chi_{j+\frac{1}{2}}$ used here are (Langdon *et al*, 1983, Eqs. (28ab))

$$\chi_{j+\frac{1}{2}} = \tfrac{1}{2}\left[\chi_j + \chi_{j+1}\right] \qquad (II.13a)$$

$$\text{or } \chi_{j+\frac{1}{2}} = \max\left(\chi_j, \chi_{j+1}\right), \qquad (II.13b)$$

$$\text{where } \chi_j = \Delta t^2 \sum_s \left[\beta\tilde{\rho}_{j,n+1}\frac{q}{m}\right]_s \qquad (II.14)$$

is a sum over species index s. In both (II.12) and (II.14), $\tilde{\rho}_{j,n+1}$ is given by (II.4).

In terms of the field

$$E_{j,n+1} = \tfrac{1}{2}\left[E_{j-\frac{1}{2},n+1} + E_{j+\frac{1}{2},n+1}\right] \qquad (II.15)$$

formed from E at half-integer positions, the particle acceleration is evaluated at $\tilde{x}_{n+1}$ using (II.6). This algorithm is the shortest implicit PIC scheme we have seen, and was the most robust in the test problem of Section II.B.1.

4. General electrostatic case

We return to the multidimensional case, possibly including a magnetic field imposed by external currents, showing the calculational steps to be performed in the two cases resulting from the choice of (I.10) or (I.11). We begin by restating the method in a more general form.

Evaluation of the extrapolated densities.

The extrapolated charge density $\rho^{(0)}_{n+1}$ is evaluated as in (I.2), but from positions $\{x^{(0)}_{n+1}\}$ obtained from the equation of motion with a_{n+1} given by $E^{(0)}_{n+1}$, which is a guess for E_{n+1}. This charge density does *not* correctly correspond to the field $E^{(0)}_{n+1}$; that is, $\nabla\cdot E^{(0)}_{n+1} \neq \rho^{(0)}_{n+1}$. We wish to calculate an improved field E_{n+1} with which the particles are re-integrated to positions $\{x_{n+1}\}$, whose charge density ρ_{n+1} does satisfy

$$\nabla\cdot E_{n+1} = \rho_{n+1} \qquad \text{(II.16)}$$

To this end we rewrite (II.16) as

$$\nabla\cdot\delta E_{n+1} - \delta\rho_{n+1} = \nabla\cdot E^{(0)}_{n+1} - \rho^{(0)}_{n+1}. \qquad \text{(II.17)}$$

where $E_{n+1} = E^{(0)}_{n+1} + \delta E_{n+1}$, and similiarly for ρ_{n+1}; $\delta\rho_{n+1}$ is due to the increments $\{\delta x\}$ in the particle positions, which in turn are due to the difference between E_{n+1} and $E^{(0)}_{n+1}$.

Evaluation of the increments due to future fields.

Using (II.10) and the equation of motion, we express $\delta\rho_{n+1}$ as a linear functional of δE_{n+1}. In the general case, the increments $\{\delta x,\delta v\}$ are evaluated by linearization of each equation of motion (Langdon *et al*, 1983; Barnes *et al*, 1983b) about position $x^{(0)}_{n+1}$; here, we have

$$\delta x_{n+1} = \delta v_{n+\frac{1}{2}}\Delta t,$$

$$\delta v_{n+\frac{1}{2}} = \frac{q\Delta t}{2m}\delta E_{n+1}(x^{(0)}_{n+1}) \qquad \text{(unmagnetized)},$$

$$\text{or} \quad \delta v_{n+\frac{1}{2}} = T\cdot\frac{q\Delta t}{2m}\delta E_{n+1}(x^{(0)}_{n+1}) \qquad \text{(magnetized)}, \qquad \text{(II.18)}$$

where $T \equiv \frac{1}{2}[I+R_n(x^{(0)}_{n+1})]$, which follows from (I.14).

With (II.18), the implicit term $\delta\rho = -\nabla\cdot(\rho\delta x^{(0)}_{n+1})$ in (II.17) is seen to be

$$\delta\rho = -\nabla\cdot(\rho^{(0)}_{n+1}\delta x) = -\nabla\cdot\left[\sum_s \frac{\rho^{(0)}_{n+1,s}q_s\Delta t^2}{2m_s}\,T_s\right]\cdot\delta E \qquad \text{(II.19)}$$

$$= -\nabla\cdot(\chi\cdot\delta E)$$

The [...] is a sum over *species* s, not each particle. If only the electrons are implicit, only they appear in (II.19). In this case, the terms [...] require only a knowledge of the electrons' ρ (in addition to the *net* ρ used on the right side of (II.21)). In general, it is sufficient to accumulate $\rho^{(0)}_{n+1,s}$ separately from species with differing q/m. This requires more storage, but *no more computation* than for an explicit code.

The implicit susceptibility

$$\chi = \left[\sum_s \frac{\rho^{(0)}_{n+1,s} q_s \Delta t^2}{2m_s}\ T_s\right] \qquad (II.20)$$

is a *tensor* due to the rotation R induced by B. The more general expression

$$\chi = \sum_s \left[\ \omega_p^2\ \frac{\partial x_{n+1}}{\partial a_{n+1}}\right]_s$$

includes equations of motion altered e.g. to include collisions. Elastic collisions of electrons on ions may be modelled by adding to the equation of motion a random rotation in the Galilean frame in which the mean ion velocity is zero. The momentum change must be added to the ions.

We now have everything needed to write an equation for $E = -\nabla\delta\phi$. On substituting our expressions for $\rho^{(0)}_{n+1}$ and $\delta\rho$ into the field equation (II.17) we have our electrostatic implicit field equation

$$\nabla\cdot[1+\chi]\cdot\nabla\delta\phi_{n+1} = \nabla\cdot E^{(0)}_{n+1} - \rho^{(0)}_{n+1} \qquad (II.21)$$

This is an elliptic field equation whose coefficients depend directly on particle data accumulated on the spatial grid in the form of an effective linear susceptibility. The rank of the matrix equation is determined by the number of field quantities defined on the zones; it is independent of the number of particles and normally is much smaller.

The field corrector (II.21) can also be expressed in terms of time filtered quantities (Barnes *et al*, 1983b). In this representation, the time filtered $\bar{\phi}^{(0)}$ and $\bar{\rho}^{(0)}$ appear on the right and the adjustment $\delta\bar{\phi}$ to $\bar{\phi}$ on the left.

This formalism guides successful implementation of spatial smoothing (Langdon *et al*, 1983; Barnes *et al*, 1983b). If spatial smoothing, denoted by the operator $\hat{S}$ is to be applied to ρ and ϕ on the grid, then $\hat{S}$ must be included in χ if the field solution is to take this into account. In some applications, this has been essential (Sections II.B.2 and II.B.3). Inconsistent smoothing has consequences to linear stability (Section II.C.4).

Advancing the Particles

The field E_{n+1} is evaluated at positions $\{x^{(0)}_{n+1}\}$ in (I.5) in integrating the particles to their final positions $\{x_{n+1}\}$. The error resulting from this approximation, and from the linearization of $\delta\rho$,

introduces a possible limitation on Δt that depends on field and density gradients; see section II.C.1.

After advancing each particle to position $\mathbf{x}_{n+1}$, one can immediately calculate its $\tilde{\mathbf{x}}_{n+2}$ and its contribution to $\tilde{\rho}_{n+2}$. In this way, only one pass through the particle list is required per time step, an advantage when the particles are stored on a slower memory device such as rotating magnetic disk.

5. Iterative Solution of Corrector Equation in Two Dimensions with Magnetic Field

Except for one-dimensional systems, the use of direct inversion for the solution of the field corrector equation (II.21) requires an impractically large amount of computer time and memory. Global iterative methods (Concus and Golub, 1973; Nielson and Lewis, 1976; Busnardo-Neto *et al*, 1977) are effective for the inversion of variable coefficient elliptic operators of the type (II.21). Other successful methods include preconditioned conjugate gradient for asymmetric operators (Kershaw, 1978; Petravic and Kuo-Petravic, 1979; Kershaw, 1980), "dynamic ADI" (Doss and Miller, 1979), and "multigrid adaptive" methods (Brandt, 1977); see also Brackbill and Forslund (1984).

The variable coefficient operator is approximated by a simpler operator whose inverse may be obtained directly. In global iteration techniques, this approximate inverse is applied to the residual (difference between right and left hand members) of the full elliptic equation. The adjustment to the solution is used to change the residual. If the approximate operator is chosen judiciously, convergence of the residual to an acceptably small value will occur in a few iterations.

The simplest such scheme for (II.21) is obtained by replacing the variable χ by a constant tensor χ_0 (Barnes and Kamimura, 1982; Tajima and LeBoeuf, 1981). The resulting constant coefficient operator may be directly inverted using Fast Fourier Transform techniques. It is natural to choose χ_0 to be the average value of χ over the domain, however, this choice leads to divergence of the iteration for certain density profiles. A more reliable choice, suggested by Concus and Golub (1973) is to choose χ_0 corresponding to the average of the maximum and the minimum densities. Thus, χ_0 is taken as

$$\chi_0 = \tfrac{1}{2}(\rho_{e,max} + \rho_{e,min})\sum_j \chi_j / \sum_j \rho_{e,j} \qquad (II.22)$$

The global iteration then proceeds by defining the residual as

$$\epsilon = \nabla^2\phi^{(0)} + \rho^{(0)} + \nabla\cdot[1+\chi(x)]\cdot\nabla\delta\phi_m \qquad (II.23)$$

where m is the iteration index. The iteration equation is obtained using the approximate operator as

$$-\nabla\cdot[1+\chi_0]\cdot\nabla[\delta\phi_{m+1}-\delta\phi_m] = \epsilon_m \qquad (II.24)$$

Equation (II.24) is easily inverted by Fourier transforming. If k is the Fourier transform variable, the iteration may be represented as

$$\delta\phi_{m+1}(k) = \delta\phi_m + \epsilon_m(k)/[k^2+k\cdot\chi_0\cdot k] \qquad (II.25)$$

After $\delta\phi_m$ is replaced by $\delta\phi_{m+1}$, the residual is recomputed and convergence is tested by computing the maximum of ϵ_{m+1} over the mesh. It is convenient to use a combination of x and k space to compute ϵ_{m+1}. The constant coefficient part, $\nabla^2\delta\phi_{m+1}$, may be evaluated in k space. The nonconstant coefficient part is evaluated by transforming $\delta\phi_{m+1}$ to x space, multiplying by χ and transforming back to k space. If χ contains a smoothing operator $\hat{S}$ this is applied in k space and also included in χ_0.

The global iteration described here has been shown to be convergent and efficient in a number of applications (Barnes *et al*, 1983a; Barnes *et al*, 1983b). Some applications are described in Section II.B.

6. Comparison to the "Moment" Method

The field predictor (II.11) has some features in common with the field predictor in the moment method. This is not surprising since both methods attempt an approximate solution of similar equations. The relation of terms arising in the implicit moment and direct implicit viewpoints is discussed by Mason (1984) and Langdon *et al* (1983); here we summarize and comment briefly.

The counterpart to χ in the moment method is approximated from the density ρ_n rather than being formed from $\tilde{\rho}_{n+1}$ or $\rho^{(0)}_{n+1}$. The source term $\tilde{\rho}_{n+1}$ in (II.11) is replaced by ρ_n plus the divergence of current and stress tensor terms. If there could be no finite-difference errors, this combination would equal $\tilde{\rho}_{n+1}$. These approximations result in a stability constraint $kv_t\Delta t \lesssim 1$ or $k\bar{v}\Delta t \lesssim 1$ (Section II.C.1) that does not arise in the direct method, as well as requiring more computation.

We believe that the particle equations themselves are a better guide to the zero-order state than are the moment equations.

As moment and direct codes are borrowing features from each other, the distinction becomes more that of viewpoint in deriving algorithms and less in the resulting codes themselves. Experience with moment codes using ad hoc spatial differencing encouraged experimentation with simpler differencing in direct codes. Insight gained from the direct method shows how to eliminate the stress tensor which contributes to the $kv_t\Delta t$ constraint in moment codes (Brackbill and Forslund, 1984). Design of optimal codes requires understanding the fruits of both viewpoints.

II.B. Representative results

1. Free expansion of a plasma slab

Denavit (1981) used the one-dimensional expansion of a plasma slab as as one check on his early moment-method code. Featuring sharp gradients initially and a large range of density, this problem is also used to check and improve variations of direct-method algorithms. Friedman *et al* (1981) emphasize best performance in a one-dimensional electrostatic implementation. Langdon *et al* (1984), as outlined here, sought to isolate those forms most suitable for extension to a two-dimensional and electromagnetic code. Without resorting to spatial smoothing, adequate accuracy and robust behavior were obtained. Smoothing makes the field equation more expensive to solve, and the resulting loss of resolution may be too costly in 2d. With $n\Delta x = 64$ particles per cell in the slab initially, and values of $\omega_{pe}\Delta t$ as large as 120 (much larger than have been reported previously for unmagnetized plasma), they find that two parameters measure the stress on the algorithm.

The more important parameter is $\chi_1 = \beta q^2\Delta t^2/m|\Delta x|$, where q and m are the particle charge and mass, and $|\Delta x|$ is the zone volume. This is a worst-case measure of the validity of linearization in the field prediction, as stressed by short-wavelength sampling fluctuations in the charge density. Using the simplified algorithm of Section II.A.3 with either (II.13a) or (II.13b), they obtain reasonable results with χ_1 well over 100. Most other variants, including the momentum-conserving algorithm (Section II.C.2), suffer nonlinear numerical instability at the edge of the expansion when $\chi_1 \gtrsim 1$.

With χ_1 written as $\beta(\omega_{pe}\Delta t)^2/N_c$, where N_c is the number of particles per cell ($n\Delta x$ in one dimension), the value of being able to run with $\chi_1 >> 1$ is clarified. Many applications of two-dimensional explicit codes require only $N_c \gtrsim 10$. If we were restricted to $\chi_1 \lesssim 1$,

we would need a number of particles per cell exceeding $(\omega_{pe}\Delta t)^2$, which would be a severe limitation.

The second parameter is $v_t\Delta t/\Delta x$, the ratio of thermal electron transit distance per cycle to the zone size. With $v_t\Delta t/\Delta x > 1$, energy conservation is degraded in the absence of spatial smoothing. The ability of a direct-implicit code to remain stable is useful with nonuniform meshes where some cell dimensions may be much smaller, and helps evade failures due to uninteresting transients or small regions.

2. Ion-acoustic fluctuations of a nonequilibrium plasma

The ion-acoustic fluctations of a uniform thermal, unmagnetized, two-temperature, one-dimensional plasma are examined (Barnes *et al*, 1983b). Since the ion-acoustic fluctuations represent an extremely small part of the total fluctuation energy of a thermal plasma and are strongly affected by electron Landau damping in the parameter range studied, these results represent a severe test of the applicability of the model.

Plasma parameters for the case shown here were; electron Debye length $\lambda_D = 0.05$, mass ratio $m_i/m_e = 100$, temperature ratio $T_e/T_i = 20$, initial electron and ion densities are equal and uniform. The numerical parameters used were; cell size $\Delta x = 1$, system length $L_x = 128$, number of particles of each species $N_0 = 9216$. Periodic boundary conditions were taken and the particle shape, introduced as a smoothing of grid quantities, was given by a Gaussian $\hat{S}(x) = \exp(-r^2/2a^2)/a(2\pi)^{\frac{1}{2}}$, with $a = 3\Delta x$. The time step was fixed at $\omega_{pe}\Delta t = 10$, a factor of 50-100 over that possible for an explicit algorithm.

Simulation results are summarized in Figs. 1 and 2. The time evolution of the total energy normalized to its initial value is shown in Fig. 1. A very slow cooling of the plasma is observed. The total energy loss is less than 10% over the time interval $\omega_{pe}t=0.0-1.0\times10^5$. The physical cooling rate of the electrons onto the ions is much larger for the simulation parameters than the numerical rate (Barnes *et al*, 1983b).

The collective behavior of the plasma at frequencies $\omega<<\omega_{pe}$ is displayed in Fig. 2. The time-averaged electrostatic energy per degree of freedom, $k_BT_e/2$ (k_B is Boltzmann's constant), or fluctuation spectrum, is shown in the figure.

A stringent test of the electron response at low frequencies is afforded by comparison of the simulation results with theory. If the resonant electron response is retained by the direct method, the fluctuation spectrum will be given by the upper curve in Fig. 2. If the

low-frequency electron response is only adiabatic, the lower curve is predicted. The ratio of the former to the latter is approximately T_e/T_i. The simulation spectrum indicated by dots closely follows the prediction including resonant electron response. Note also that the wavenumbers with maximum energy observed in the simulation and predicted by theory agree exactly. At larger wavenumbers, the theory is questionable because of approximations made in the derivation.

In summary, the fluctuation spectrum indicates that the resonant electron response at low frequencies is described accurately by the implicit method. It is also clear from these results that fluctuations at mode frequencies higher than the ion-acoustic range have been suppressed; otherwise the spectrum would have been nearly flat in this frequency range.

3. Gravitational interchange instability of a magnetized plasma

Using the direct method, and treating both the electrons and ions as zero gyroradius particles using the method described in Section III (with gyroradius effects neglected), a two-dimensional magnetized plasma is examined. An unstable gravitational interchange is studied for an inhomogeneous plasma. This calculation is carried out for system size $L_x = L_y = 32\Delta x$, number of particles $N_0 = 4608$, mass ratio $m_i/m_e = 100$, electron cyclotron frequency $\Omega_e = \omega_{pe}$, and $a=3\Delta x$ in the Gaussian shape factor $\hat{S}$. The magnetic field is normal to the simulation plane.

Electrons and ions are loaded initially with their guiding center velocity $V_\perp = 0$ in such a way that the distribution of particles is uniform in the left half of the simulation domain. No particles are loaded in the right half of the domain. A gravitational acceleration to the right drives an unstable interchange localized near the interface at the middle of the domain.

The effect of the polarization motion of the ions is very important for this high-density plasma ($\omega_{pi}/\Omega_i >> 1$). If the polarization motion is neglected, the growth rate becomes unphysically large for high density. For the simulation parameters considered here, the physical growth rate is 1/7 the growth rate found neglecting polarization.

In the simulation, the global iteration method described above is used and an extremely large time step of $\omega_{pe}\Delta t = 10^3$ is used. Simulation results for an appropriate gravitational acceleration are summarized in Figs. 3 and 4. In this case the plasma is initially perturbed with the longest y wavelength so that the growth rate of a single mode may be more accurately measured. In Fig. 3, the electrostatic field energy is shown in a semi-log plot as a function of

time. The observed growth rate is within 15% of the theoretically predicted value, verifying the correct modelling of ion polarization motion.

Figure 5 shows three different snapshots of the ion density contours. The positions of roughly 10^3 of the ions are also shown as points in the figure. As can be seen, the unstable interface near the middle of the simulation domain evolves through a linear growth stage, toward a nonlinear "spike and bubble" stage. The only saturation mechanism is provided by the finite size of the periodic simulation domain. Thus, plasma leaving on the right (left) reenters on the left (right). In this way, the configuration evolves toward a state of nearly steady flow with constant potential driving stationary vortices.

II.C. Properties of Implicit Particle Codes

1. Remaining limitations on time step

Although we have overcome the stability limit on $\omega_{pe}\Delta t$, there remain restrictions which involve Δt. In addition to the aspects discussed under the following subheadings, Sections II.C.3 and II.C.4 are also relevant.

Doppler frequency limit

When a particle moves in one time step a distance greater than a scale length L for spatial variation of fields, the particle does not sample the field sufficiently closely in space to respond accurately to the field structure. In analysis, this is stated in terms of the Doppler-shifted frequency $\omega - \mathbf{k}\cdot\mathbf{v}$. If the thermal spread of electron velocities, $v_t = (T_e/m_e)^{\frac{1}{2}}$, and wavenumber k are such that $kv_t\Delta t \gtrsim 1$, then the Doppler-shifted frequency exceeds Δt^{-1} for a large fraction of the electrons. It is not surprising that the collective response is qualitatively incorrect, showing an excess of shielding, as indicated by the dielectric function becoming

$$\epsilon \cong 1 + \beta\omega_{pe}\Delta t^2 + (\text{ion response}) \qquad \text{(II.26a)}$$

instead of the correct result,

$$\epsilon \cong 1 + (k\lambda_D)^{-2} + (\text{ion response}) \qquad \text{(II.26b)}$$

Violation of the restriction $kv_t\Delta t \lesssim 1$ in direct-method electrostatic codes does not in general result in instability. In many applications, the sharp field gradients may arise only during time intervals, or in spatial regions, such that the inaccuracy does not

interfere with the purpose of the simulation. In contrast, strong instability which has been observed with the moment method has been traced to a constraint on $kv_t\Delta t$ (Sakagami *et al*, 1981; Denavit, private communication) and is attributed to lack of convergence (Denavit, 1981; Cohen *et al*, 1982a). Such instability, as opposed to innocuous inaccuracy, is disruptive to the simulation.

The Doppler frequency, or transit time, limit is analyzed by Langdon (1979a), Denavit (1981), Cohen *et al* (1982b), Langdon *et al* (1983), and references therein. See also Sections II.B.1 and II.C.4 of this Chapter.

Limits due to field and density gradients

Linearization of the time-advanced charge density breaks down when field or density gradients are too large. Nonetheless, the codes have been made to function successfully, but convergence is not guaranteed.

Evaluation of $\delta\mathbf{x}$ in terms of $\mathbf{E}_{n+1}$ at $\mathbf{x}_{n+1}^{(0)}$ rather than at $\mathbf{x}_{n+1}$ creates a error $\cong \delta\mathbf{x}\cdot\nabla\mathbf{E}$. Denavit (1981) interprets this term in terms of the frequency of oscillation of a particle trapped in a local potential minimum. The relative error is $\beta(\omega_{trap}\Delta t)^2$. To compare the severity of this and the transit-time limitations, note that

$$\beta(\omega_{trap}\Delta t)^2 = \beta(kv_e\Delta t)^2\ q\phi/T_e \qquad (II.27)$$

Thus, if we take $kv_e\Delta t \lesssim 1$ as given, the linearization is justified if $q\phi \lesssim T$. Put another way, if $kv\Delta t \lesssim 1$, then $(\omega_{trap}\Delta t)^2 = ka\Delta t^2$ is small if $a\Delta t$, the impulse in one time step, is small compared to v. In grossly nonneutral regions, where the net charge $\Delta\rho$ is comparable to the electron charge ρ_e,

$$\beta(\omega_{trap}\Delta t)^2 \cong (\omega_{pe}\Delta t)^2\ \Delta\rho/\rho_e \qquad (II.28)$$

will not be small unless $\omega_{pe}\Delta t$ is small in that region.

A similar limit due to magnetic field gradient can be interpreted as $(\omega_\beta\Delta t)^2 \lesssim 1$, where ω_β is the "betatron frequency".

The expression $\delta\rho = -\ \nabla\cdot(\rho\delta\mathbf{x})$ is valid when $\delta\mathbf{x}$ is smaller than density gradient scale lengths.

The validity of linearization is treated by Denavit (1981), Langdon *et al* (1983), Cohen *et al* (1984), and references therein, and in Section II.B.1 of this Chapter.

2. Momentum Conservation

Properties of the physical system can often be reproduced exactly in the simulation, even though the governing equations are not solved exactly. Momentum conservation is easily arranged for in explicit electrostatic simulations. Here we show how to carry this property over to implicit simulation.

Referring to Section II.A, we see from (II.4) and (II.6) that the net particle acceleration can be written

$$\sum_i m_i a_{i,n+1} = \Delta x \sum_j \tilde{\rho}_{j,n+1} E_{j,n+1} \tag{II.29}$$

In explicit codes, in the analogous sum $\Delta x \sum \rho E$, E is the solution with ρ as source. The question of momentum conservation is then confined to the symmetry properties of the partial differential equations and the boundary conditions. Momentum conservation is easily obtained where expected physically, at least with Cartesian meshes.

The same would be true in an implicit code if we solved the field and particle equations exactly, but we do not. In (II.29), $E_{j,n+1}$ corresponds not to $\tilde{\rho}_{j,n+1}$ but to

$$-(\nabla^2\phi)_{j,n+1} = \tilde{\rho}_{j,n+1} + \delta\rho_j = \sum_i q_i \left[S(X_j - \tilde{x}_{i,n+1}) - \delta x S'(X_j - \tilde{x}_{i,n+1}) \right] \tag{II.30}$$

with δx given by (II.7). So, if we revise (II.6) to

$$m_i a_{i,n+1} = \Delta x q_i \sum_j E_{j,n+1} \left[S(X_j - \tilde{x}_{i,n+1}) - \delta x S'(X_j - \tilde{x}_{i,n+1}) \right] \tag{II.31}$$

where [..] is the same as in (II.30), and if the Poisson equation (II.8) is solved exactly, then ρ and E correspond, and momentum is conserved when appropriate physically.

Let us interpret (II.31) as two steps in the particle mover. First, evaluate an interim position

$$\begin{aligned} x'_{i,n+1} &= \delta x_i + \tilde{x}_{i,n+1} \\ &= \beta \Delta t^2 (q_i/m_i) \Delta x \sum_j S(X_j - \tilde{x}_{i,n+1}) E_{j,n+1} + \tilde{x}_{i,n+1} \end{aligned} \tag{II.32}$$

using (II.7) for δx. Then, evaluate a at position x' using an expansion of (II.6) about $\tilde{x}_{n+1}$, which is (II.31). This $a_{i,n+1}$ is used for the final values of $v_{n+\frac{1}{2}}$ and x_{n+1}. The source term for Poisson's equation,

$\tilde{\rho}+\delta\rho$, is a representation of the density of positions $\{x'\}$ at which the field is evaluated; this makes momentum conservation possible.

We can retain momentum conservation while simplifying the field equation by using a simpler expression for δx in forming the field equation (II.30) and in moving the particles, (II.32). For example, we can replace (II.7) by

$$\delta x_i = -\beta\Delta t^2(q_i/m_i)\Delta x\sum_j S_0(X_{j+\frac{1}{2}}-\tilde{x}_{i,n+1})\ \frac{\phi_{j+1,n+1}-\phi_{j,n+1}}{\Delta x} \qquad (II.33)$$

where S_0 is the nearest-grid-point (NGP) weighting function. If the function S used in (II.30) and (II.31) is the linear spline, S_1, then (II.30) becomes a tridiagonal field equation for ϕ, instead of the pentadiagonal equation found with strict differencing. When integrating the particles, the interim position (II.32) is also modified to use S_0. The field equation can be written

$$\tilde{\rho}_{j,n+1} = \left[(1+\chi_{j+\frac{1}{2}})E_{j+\frac{1}{2},n+1} - (1+\chi_{j-\frac{1}{2}})E_{j-\frac{1}{2},n+1}\right]/\Delta x, \qquad (II.34)$$

$$\text{with } E_{j+\frac{1}{2},n+1} = -\frac{\phi_{j+1,n+1}-\phi_{j,n+1}}{\Delta x} \qquad (II.35)$$

$$\text{and } \chi_{j+\frac{1}{2}} = \sum_i \beta\Delta t^2(q_i^2/m_i)\ S_0(X_{j+\frac{1}{2}}-\tilde{x}_{i,n+1}) \qquad (II.36)$$

$$\text{from which } E_{j,n+1} = \tfrac{1}{2}\left[E_{j-\frac{1}{2},n+1} + E_{j+\frac{1}{2},n+1}\right] \qquad (II.37)$$

[Equations (II.33)-(II.37) are the same in one dimension as for the Hamiltonian algorithm (Langdon, Cohen and Friedman, 1983, Section 4.2)] This scheme is almost as simple as that in section II.A.3.

This topic was first treated by Friedman *et al* (1983), who extend the treatment to include spatial smoothing.

Note that momentum conservation cannot be contrived for the formulation of Barnes *et al* (1983b), because time filtering of mesh variables destroys Galilean invariance.

3. Energy Conservation and Artificial Cooling

To understand better the origins and control of nonphysical cooling (a manifestation of error in codes using damped equations of motion (Adam *et al*, 1982; Barnes *et al*, 1983b), the Lenard-Balescu collision operator corresponding to implicit time integration is examined. We find two spurious terms due to phase errors associated with damping. One is a nonresonant contribution to the polarization drag. The other is a spurious nonresonant contribution to dynamical friction and corresponds to the drag calculated by Cohen *et al* (1982b) but with the field given by the thermal fluctuation spectrum.

Quantitative calculations of cooling rates based on the kinetic theory described here have not yet been carried out. However, cooling rates observed in simulations of thermal plasmas (Barnes, *et al.*, 1983b) indicate that cooling is likely dominated by damping of a broad band of thermal fluctuations. Thus, the reduction in cooling for schemes with third-order damping compared with those with first-order damping is much less than the reduction in the damping of low-frequency plasma modes. The cooling rate is reduced when the number of modes is increased, decreasing the fluctuation energy per mode. Further, the most effective means of reducing cooling is to cut the width of the fluctuation spectrum by cutting off in wavenumber (spatial smoothing) or in frequency (by increasing Δt). Finally, acceptably low cooling rates may be obtained in a third-order damping scheme with a moderate amount of spatial smoothing.

Kinetic Theory

The kinetic theory is based on Birdsall and Langdon (1984), Chapters 9 and 12. Here we neglect the effects of the spatial grid. In the Fokker-Planck collision operator (Balescu-Lenard equation) corresponding to implicit time integration, the velocity diffusion is not altered in any interesting way, but the velocity drag terms are.

Polarization Drag

One part of the drag, due to anisotropic polarization of an unmagnetized plasma by the test particle, in a Galilean-invariant code (e.g. using Eqs. (I.9-I.10), is

$$\langle a \rangle_{pol} = \frac{q^2}{m} \int \frac{dk}{(2\pi)^3} \frac{k}{k^2} \mathrm{Im} \frac{1}{\epsilon(k, k\cdot v)} \qquad \text{(II.38)}$$

$$= -n_0 \frac{q^4}{m^2} \int \frac{dk}{(2\pi)^3} \frac{k}{k^2} \int dv' \; \frac{f(v')}{|\epsilon(k,k\cdot v)|^2} \; \mathrm{Im}\left(\frac{X}{A}\right)_{k\cdot(v-v')+i0}$$

(in rationalized cgs units), in which

$$\epsilon(k,\omega) = 1 + \omega_p^2 \int dv \; f_0(v) \; \left(\frac{X}{A}\right)_{\omega-k\cdot v+i0} \qquad \text{(II.39)}$$

where $(X/A)_{\omega-k\cdot v+i0}$ is the ratio of Fourier amplitudes of $x^{(1)}$ and $a^{(1)}$ resulting from the finite-difference equation of motion (and would be $-(\omega-k\cdot v+i0)^{-2}$ for exact integration), and $\epsilon(k,\omega)$ is the corresponding dielectric function. The meaning of the term "+i0" is that $(..)_{\omega+i0}$ is understood to mean the limit of $(..)_{\omega+i\gamma}$ as γ approaches zero through *positive* values. Normally $\mathrm{Im}(X/A)_{\omega-k\cdot v+i0} = -\pi\delta'(\omega-k\cdot v)$ which leads to the resonant (Landau) contribution, but here $\mathrm{Im}(X/A)_{\omega-k\cdot v+i0}$ is *also* nonzero for $\omega-k\cdot v \neq 0$ due to phase errors associated with numerical damping.

"Dynamical Friction"

The other part of the drag, the "dynamical friction" can also be expressed in terms of Im(X/A):

$$\langle a \rangle_{fluct} = \frac{q^2}{m^2} \int \frac{dk}{(2\pi)^3} \frac{d\omega}{2\pi} \; k\cdot(EE)_{k,\omega} \; \mathrm{Im}\left(\frac{X}{A}\right)_{\omega-k\cdot v+i0} \qquad \text{(II.40)}$$

where $(EE)_{k,\omega}$ is the fluctuation spectrum. This result corresponds to that in Section 5 of (Cohen *et al*, 1982b), in which the field consisted of a single wave rather than a spectrum. Here we use the thermal fluctuation spectrum (Langdon, 1979b; Birdsall and Langdon, 1984)

$$(EE)_{k,\omega} = \frac{\kappa\kappa}{K^2} \; (\rho^2)_{k,\omega} \qquad \text{(II.41)}$$

$$(\rho^2)_{k,\omega} = \frac{2\pi\rho_0 q}{|\epsilon(k,\omega)|^2} \int dv \; f_0(v) \sum_q \delta(\omega-k\cdot v-q\omega_g) \qquad \text{(II.42)}$$

where $\omega_g \equiv 2\pi/\Delta t$, and κ, K^2 express ratios between the quantities ρ, ϕ and E defined on the grid, thusly: $E = -i\kappa\phi$, $\rho = K^2\phi$ (rationalized cgs units). As a check on the theory, we can verify that the expressions (II.38) and (II.40), with the thermal spectrum, together conserve momentum of the overall distribution of particles.

Energy Loss (Cooling)

The Fokker-Planck equation describing the evolution of the velocity distribution function f(v) is

$$\frac{\partial f}{\partial t} = \frac{\partial}{\partial v}\cdot\left[- f\langle a\rangle_{pol} - f\langle a\rangle_{fluct} + \frac{\partial}{\partial v}\cdot fD\right] \qquad (II.43)$$

where D(v) is the diffusion tensor. Because the resonant parts of (II.38) and (II.40) cancel, (II.43) conserves energy with continuous time. We can compute the rate of cooling due to the nonresonant part of numerical origin:

$$\frac{d}{dt}K.E. = \int dv\ v\cdot\langle a\rangle\ f(v) = -\tfrac{1}{2}n_0\frac{q^4}{m^2}\int\frac{dk}{(2\pi)^3}\frac{1}{k^2}\int dvdv'\ f(v)f(v')$$

$$\times\left[\frac{1}{|\epsilon(k,k\cdot v)|^2} + \frac{1}{|\epsilon(k,k\cdot v')|^2}\right] k\cdot(v-v')\ \mathrm{Im}\left(\frac{X}{A}\right)_{k\cdot(v-v')} \qquad (II.44)$$

where it is now to be understood that the resonant part of Im(X/A) is dropped. For the C_1 equation of motion scheme, $\mathrm{Im}(X/A)_\omega = c_1\Delta t^2\sin\omega\Delta t$, while for the D_1 scheme, $\mathrm{Im}(X/A)_\omega = \Delta t^2\sin\omega\Delta t/(5-4\cos\omega\Delta t)$ (Cohen *et al*, 1982b). In both cases, if the spread in particle velocities is less than $\pi/k_{max}\Delta t$ then the integrand is always positive so only cooling results. This is true quite generally for damped time integration, including explicit integration (Adam *et al*, 1982).

For these schemes with 3rd-order damping, the last two factors in the integrand together are proportional to $[k\cdot(v-v')\Delta t]^2$ for small values. With first-order damping, this approaches a nonzero constant instead (Cohen *et al*, 1982b). Other implementations of third-order schemes, e.g. Barnes *et al* (1983b), produce different phase errors and hence different cooling rates.

We hope that application of this analysis will lead to insight into control of errors in implicit simulation.

4. Effects of imperfect field solution on linear stability and dispersion

Analysis of linear stability and dispersion in uniform plasma, as described by dispersion relations, provides guidance to permissible simplifications of the field solution. Generically, these relations are of the form

$$K^2(k)\epsilon(k,\omega)\phi = ([\nabla\cdot\chi\nabla]_{code} - [\nabla\cdot\chi\nabla]_{strict})_k\delta\phi \qquad (II.45)$$

where [...] are the Fourier transforms of the $\nabla\cdot\chi\nabla$ operator, in uniform plasma; "strict" and "code" refer to the rigorous representation of Section II.A.2 and to the representation used in the code; K^2 is the ratio ρ/ϕ; $\delta\phi$ is the transform of $\phi_{n+1} - \phi_{n+1}^{(0)}$; $\epsilon(k,\omega) = 0$ is the dispersion relation applicable to *exact* solution of the implicit, finite-differenced particle and field equations. Expressions for ϵ for warm plasma, including exactly the effects of Δx and Δt, have been published (Langdon, 1979a). It is assumed that iteration over the particles is not in use. Here we show some contributors to the right-hand-side of (II.45) and some qualitative consequences, but do not attempt an encyclopaedic enumeration of the possibilities.

Far from being relevant only to direct-method codes, similar, but more complex, methods and results arise with moment-method codes (Denavit, 1981).

Non-strict differencing and inconsistent filtering

For the one-dimensional simplified algorithm (Section II.A.3),

$$\epsilon(k,\omega)\phi = -\beta(\omega_p\Delta t)^2\sin^2(k\Delta x/2)\ \delta\phi \qquad (II.46)$$

If smoothing of ρ or ϕ is used without being included in the susceptibility term we find, now ignoring the spatial grid,

$$\epsilon(k,\omega)\phi = -\beta(\omega_p\Delta t)^2(1-\hat{S}^2)\ \delta\phi \qquad (II.47)$$

Spatial differencing and/or smoothing also modify ϵ.

With $\phi_{n+1}^{(0)} = 0$, $\delta\phi = \phi$. The $\delta\phi$ terms do not upset linear stability (assuming $\hat{S} \leq 1$). On the other hand, with $\phi_{n+1}^{(0)} = \phi_n$, the phase of $\delta\phi/\phi = (1 - z^{-1})$ is destabilizing in the above examples. Such analysis provides guidance among the many possibilities (Cohen *et al*, 1984).

Nonlocal susceptibility

In addition to the effects of simplified differencing, Barnes *et al* (1983b) acquire an additional contribution due to evaluation of E_{n+1} at x_n rather than x_{n+1} (Equation (I.11) *versus* (I.10)) without taking this into account in the susceptibility. Ignoring spatial grid effects, their $\delta\bar{\rho}$ is

$$\delta\bar{\rho}(x) = \nabla\cdot\left[\tfrac{1}{2}\rho^{(0)}_{n+1}(x)\frac{q}{m}\Delta t^2\nabla\delta\bar{\phi}(x-v^{(0)}\Delta t)\right] \qquad (II.48)$$

weighted over zero-order particle velocities $v^{(0)}$. In practice, the $v^{(0)}\Delta t$ term is dropped, a local approximation. With no iteration over the particle list and field prediction, the dispersion relation becomes

$$\begin{aligned}\epsilon(k,\omega)\bar{\phi} &= \tfrac{1}{2}(\omega_p\Delta t)^2\left[1 - \int dv\ f_0(v)e^{ik\cdot v\Delta t}\right]\delta\bar{\phi} \\ &= \tfrac{1}{2}(\omega_p\Delta t)^2\left[1 - e^{ik\cdot\bar{v}\Delta t-\frac{1}{2}(kv_t\Delta t)^2}\right]\delta\bar{\phi} \qquad (II.49)\end{aligned}$$

where f_0 is the particle velocity distribution function and the second line applies for a drifting Maxwellian. Due to the destabilizing effect of the right-hand-side, this formulation is not recommended for application to drifting plasma.

The linear dispersion errors which are responsible for this destabilization may be corrected without requiring additional particle quantities, if this is desirable. As the analysis above shows, the destabilizing phase error comes from the neglected displacement between the time n particle positions where the acceleration of Eq. (I.11) is applied, and the time n+1 particle positions which produce the time n+1 density. If the acceleration (II.11) is redefined as

$$\bar{a}_n = \frac{q}{2m}\left[\bar{E}_{n-1}(x_n-\Delta t v_{n-\frac{1}{2}}) + E_{n+1}(x_n+\Delta t v_{n-\frac{1}{2}})\right] \qquad (II.50)$$

this displacement vanishes. When the dispersion relation of this scheme, with no iteration over the particle list and field predictor, is investigated for a cold drifting beam, no linear instability is found for any value of the drift speed or time step.

III. GYRO AVERAGED PARTICLE SIMULATION (GAPS)

In this section is developed a technique useful for studying magnetized plasma phenomena which are much slower than the period of cyclotron oscillation for either or both species. In such applications, it is neither desirable nor efficient to follow the rapid gyration of individual particles about the magnetic field. Rather, the primitive equations of motion should be replaced by equations which contain only the slower time scales of interest, i.e. the transit and drift time scales.

The approach adopted here is to replace the nearly point particles which represent the fastest time scales by the gyro average of such a charge. Thus, in both the charge and force calculations, the shape factor is chosen to represent a ring of charge corresponding to the motion of a point charge during a single gyroperiod.

Such gyroaveraging leads to equations of motion which still contain the terms driving high-frequency motion. Implicit differencing of these gyroaveraged equations removes the vestiges of this unwanted high-frequency branch. The resulting model selects the solution which evolves only on the slower transit and drift time scales.

An alternative approach (Lee, 1983; Dubin *et al*, 1983) replaces the primitive physical fields with fields obtained by a several-term adiabatic Hamiltonian theory. It seems difficult to include effects of spatially inhomogeneous magnetic geometries in this alternate approach. The techniques described in this section may be applied to arbitrary geometries if the gyroradius is taken small but finite (Barnes and Kamimura, 1982). The case of strong inhomogeneity and large $k_\perp r_l$ (where $k_\perp$ is the wave number perpendicular to the magnetic field and r_l a typical gyroradius) seems difficult to treat satisfactorily. Some comments on these difficulties are given at the end of this section.

The properties of GAPS are developed for the simplest case: the magnetic field B is assumed uniform and the electric field E is assumed electrostatic ($\nabla \times E = 0$). First, the motion of individual simulation particles, representing guiding center positions, are considered. Then the implementation of GAPS is shown to depend on the direct method of the previous section. Some implementation details are given. Extensions to nonuniform B and to electromagnetic E are briefly indicated.

III.A Individual Particle Motion

An intuitively appealing technique for removing the fast cyclotron time scale from particle motion, is the replacement of the instantaneous

Lorentz force on a particle by its average over the fast time scale. Northrup (1961) has shown that such a procedure describes drift motion in an electromagnetic field under appropriate conditions. Such a procedure is based on the existence of an adiabatic invariant associated with the wide separation of the time scale for gyration and that for variation of the electromagnetic field.

When such an assumption is appropriate, as is supposed in the case of interest here, there exists an invariant μ given to lowest order by the magnetic moment,

$$\mu = \frac{mv_\perp^2}{2B}. \tag{III.1}$$

Thus, the particle orbit is given to lowest order by

$$x = \xi + g(\theta) \tag{III.2}$$

where ξ is the (slowly varying) guiding center position, g is the (rapidly varying) instantaneous gyrovector, and θ the gyrophase. The magnitude of g is the gyroradius $r_L = \sqrt{2\mu/q\Omega}$ and its direction rotates about B with θ. If i is any unit vector normal to B,

$$g = r_L\left[\cos\theta\ i + \sin\theta\ \frac{i\times B}{B}\right] \tag{III.3}$$

With the decomposition of Eq. III.2, the Lorentz force is replaced by its gyroaverage. Thus, the equation of motion of a simulation particle becomes

$$m_i \frac{dV_i}{dt} = \frac{1}{2\pi}\int_0^{2\pi} d\theta\, F[\xi_i + g(\theta)] + q_i V_i \times B, \tag{III.4}$$

where the B field has been assumed uniform, and $V_i = d\xi_i/dt$ is the guiding center velocity.

The gyroaveraged force may be simplified using Eq. (I.5)

$$F_{\mu i} = \frac{1}{2\pi}\int_0^{2\pi} d\theta\, F[\xi + g(\theta)] = q_i |\Delta x| \sum_j E_{\mu j} S(X_j - \xi_i), \tag{III.5}$$

where

$$E_{\mu j} = -\nabla_j \phi_\mu \tag{III.6}$$

with

$$\phi_{\mu j} = \frac{1}{2\pi} \int_0^{2\pi} d\theta \; \phi(X_j + g). \tag{III.7}$$

The gyroaveraged equation of motion (III.4) describes drift and transit motion if the proper initial conditions are chosen (Northrup, 1961). These initial conditions associate a unique perpendicular velocity $V_\perp = U_\mu(\xi, V_\parallel, 0)$ with a guiding center whose initial position is ξ and whose initial parallel velocity is $V_\parallel$. The general solution consists of the desired drift branch, a rapid perpendicular gyration about the magnetic field, and the nonlinear interaction of these two branches.

To select the desired drift solution in a difference approximation to (III.4), the initial $V_\perp$ assigned to each guiding center is chosen as close to U_μ as practical. Unwanted gyrations are avoided by the proper differencing of the last term on the right of (III.4). If the differencing of this term is modified slightly from that used in explicit plasma simulation (I.7ab), gyrations are weakly damped and the desired drift motion is recovered.

The simplest treatment is to slightly decenter the leapfrog difference equations. This leads to the difference equations

$$\frac{\xi_{n+1} - \xi_n}{\Delta t} = V_{n+\frac{1}{2}}, \tag{III.8}$$

$$\frac{V_{n+\frac{1}{2}} - V_{n-\frac{1}{2}}}{\Delta t} = a_{\mu n} + \left[\left(\tfrac{1}{2}+\gamma\right)V_{n+\frac{1}{2}} + \left(\tfrac{1}{2}-\gamma\right)V_{n-\frac{1}{2}}\right] \times \frac{qB}{mc}, \tag{III.9}$$

where $a_{\mu n} = F_{\mu n} / m$ and $\gamma > 0$ is a small decentering parameter. The effects of the dissipation and phase error introduced by decentering the V×B term are very small since only the motion perpendicular to B is affected. Since gyroaveraging effectively removes cyclotron noise, perpendicular motion is little modified by decentering.

To obtain the contribution of a simulation particle to the charge density, recall that the same particle cloud contributes to the charge as samples the force. Thus, $F_{\mu i}$ may be written as

$$F_{\mu_i} = q_i \int dx\ E(x) S_\mu(x-\xi_i), \tag{III.10}$$

where

$$S_\mu(\delta x) = \frac{1}{2\pi} \int_0^{2\pi} d\theta\ S(\delta x+g). \tag{III.11}$$

The charge density associated with a plasma of gyroaveraged particles is thus

$$\rho_c(x,t) = \sum_\mu S_\mu * q n_\mu = \sum_\mu \int dx'\ S_\mu(x-x') q n_\mu(x',t), \tag{III.12}$$

where n_μ is the number density of magnetic moments μ.

III.B The Direct Method for Electrostatic GAPS

In this section, the GAPS method is combined with the direct method to give a long time step method in which there is no restriction on the time step from either the plasma oscillation period or the cyclotron period of either species.

For small gyroradius particles, the gyroaveraged acceleration $a_{\mu n}$ is nearly a_n. In that case, Eqs. (III.8-9) are the same as the earlier equations of motion (I.7ab) for $\gamma = 0$. For $\gamma > 0$, the susceptibility is slightly modified.

As in Section II.A, the equations of motion are now linearized about a prediction $\{\xi^{(0)}_{n+1}, V^{(0)}_{n+\frac{1}{2}}\}$. Linearization of (III.8) and (III.9) gives

$$\delta\xi = \Delta t \delta V \tag{III.13}$$

$$\delta V = T_\gamma \cdot \frac{q\Delta t}{2m} S * \delta E \tag{III.14}$$

where the tensor T_γ is given by

$$(1 + \theta_\gamma^2) T_\gamma = I - \theta_\gamma \times I + \theta_\gamma \theta_\gamma \tag{III.15}$$

with $\theta_\gamma = \frac{1}{2}(1+\gamma)\Omega D t$.

Following the procedure described in Section II.A, the field corrector equation is found to be similar to that obtained previously. The susceptibility tensor is now an operator containing the gyroaveraged particle shape. The susceptibility is found from (III.14) to be the

same as that given by (II.20) with T replaced by T_γ and the addition of spatial smoothing. Thus, the methods described earlier may be used to solve the field corrector associated with a single, small-gyroradius gyroaveraged species, even for $\Omega\Delta t >> 1$.

In a warm, magnetized plasma, spatial scale lengths are such that the electron gyroradius may be neglected for low-frequency electrostatic phenomena. The ion gyroradius is not negligible, however, since fluctuations with scale size comparable to the thermal ion gyroradius are both predicted theoretically and observed experimentally. If both the electron and ion species are treated by gyroaveraged equations similar to Eqs. (III.8) and (III.9), with the explicit acceleration a_n replaced by the implicit acceleration $\bar{a}_n$, a low-frequency algorithm results in which neither the plasma frequencies nor the cyclotron frequencies constrain Δt.

In this case, however, the field corrector equation will contain the gyroaveraged ion response as part of the susceptibility. The solution of such a non-local, velocity-dependent operator equation is cumbersome. This complication is avoided by treating only the electron species implicitly according to Eqs. (III.8) and (III.9) with the zero-gyro-radius acceleration $\bar{a}_n$. The ion species may be advanced by the explicit equations (III.8) and (III.9) as written. Just as there are no ion plasma modes in a neutral plasma, there is no stability constraint on Δt associated with the time scale ω_{pi}^{-1}.

To see this, consider the case of a cold, uniform, unmagnetized plasma in which the electrons are treated implicitly and the ions explicitly. The dispersion relation is a superposition of the implicit equation (I.13) and the explicit equation (I.8)

$$1 + \omega_{pe}^2\Delta t^2 \frac{z}{(z-1)^2}\left[\frac{z^2}{2z-1} + \frac{m_e}{m_i}\right] = 0 \qquad \text{(III.16)}$$

Note that for $m_e/m_i = 0$ and $\omega_e\Delta t >> 1$, the destabilizing explicit ion response [represented by the last term on the left of Eq. (III.16)] is not sufficient to destabilize the time advancement scheme. In fact, for $m_e/m_i < 1/3$ (which is trivially satisfied) there are no unstable roots of Eq. (III.16) irrespective of the size of Δt.

This observation applies to all implicit plasma simulation algorithms. It is sufficient to implicitly advance the electrons and therefore include only their susceptibility in the field corrector equation to assure numerical stability of all plasma oscillations.

The direct electrostatic GAPS algorithm advances the electrons with the predictor-corrector method outlined in Section II above. The field

corrector equation is identical to Eqs. (II.21) and (II.20) except T is replaced by T_γ defined by Eq. (III.15) and only the electron susceptibility enters. The ions are advanced explicitly according to Eqs. (III.8) and (III.9) with the gyroaveraged acceleration $a_{\mu n}$ computed from a single gyroperiod of the ion motion in the specified B field and the self-consistent E field.

The calculation of the gyroaverages of a_n and S may be computed by substepping each ion orbit around a single gyroperiod using a fractional time step δt such that a gyroperiod is completed in 4-10 fractional steps.

A more complete development of the properties of GAPS is beyond the scope of this chapter. We remark here only that it can be shown that the guiding centers of GAPS move according to a gyroaveraged Hamiltonian. Thus, a kinetic equation may be obtained for the collisionless GAPS plasma. It may be shown that the linear dispersion relation for drift waves is recovered from this kinetic equation.

Extensions of the GAPS algorithm to inhomogeneous B and electromagnetic E are possible. In these cases, the electron gyroradius must be included to first order in the gyroradius and the gyroaveraged ion equation must include the gyroaveraged $\dot{g}\times B$ force in addition to the electric force of Eq. (III.9).

IV. ELECTROMAGNETIC DIRECT IMPLICIT METHOD

Until recently, plasma simulation including the full electromagnetic field was done with explicit differencing of both the particles and fields. The latter adds a Courant-Levy-Friedrichs time-step limitation $\Delta t < c/\lambda$, where λ is approximately the mesh spacing used for the fields. This limitation has been removed in two ways. One is to alter the field equations so that they no longer support wave propagation. A proven approach here is the Darwin, or magnetoinductive, model. Another is to use implicit differencing of the field equations. Recently, codes have used implicit differencing of both fields and particles.

Darwin codes eliminate the Courant restriction $\Delta t<c/\lambda$ by dropping Maxwell's transverse displacement current term. These "pre-Maxwell equations" eliminate electromagnetic wave propagation while retaining electrostatic, magnetostatic and inductive electric fields. The equivalence of this nonradiative approximation to the Darwin Lagrangian, which retains as much of the electromagnetic interaction as possible without including retardation, was shown by Kaufman and Rostler (1971). Nielson and Lewis (1976) provide many references for the historical development of these codes. Although these codes have used explicit

differencing for the particles, it is also possible to make an implicit Darwin code.

For applications not requiring a kinetic description of the electrons, codes using a hybrid of particle ions and fluid electrons are indicated. With Darwin and quasistatic approximations, long time scales are accessible as in a fully implicit code but with less noise (Hewett, 1980, and references therein).

Implicit fields reproduce electromagnetic wave propagation at long wavelengths ($>>c\Delta t$). At short wavelengths, the electrostatic, magnetostatic, and inductive electric fields are retained, as in a Darwin code. Implicit fields can be used with explicit particles. With implicit particles, Langmuir waves are stabilized at all wavelengths, as in a implicit electrostatic code. The electrostatic fields are accurate for wavelengths longer than the electron transit distance ($v_{te}\Delta t$). These properties make an implicit electromagnetic code attractive e.g. to modeling of intense electron flow which is subject to pinching, Weibel instability (Brackbill and Forslund, 1982), and other processes generating magnetic fields which alter the electron flow (Forslund and Brackbill, 1982).

Here we outline the Darwin algorithm and a fully implicit electromagnetic algorithm. The latter is an extension of Langdon (1983) and is being implemented by Hewett and Langdon. Barnes and Kamimura have preliminary results with their version of this algorithm.

IV.A Darwin, or Magnetoinductive, Fields

The Darwin approximation neglects the transverse displacement current $\partial E_T/\partial t$, leaving

$$c\nabla\times B = J_T = J + \frac{\partial E_L}{\partial t} \qquad (IV.1)$$

$$c\nabla\times E = -\frac{\partial B}{\partial t} \qquad (IV.2)$$

Given E_n, B_n, the particles are integrated by explicit differencing to $v_{n+\frac{1}{2}}$ and x_{n+1}. Extrapolation of $v_{n+\frac{1}{2}}$ to v_{n+1} permits collection of J_{n+1}, from which B_{n+1} is obtained, e.g. by solution of $c\nabla^2 B = -\nabla\times J$.

Unlike usual electromagnetic codes, the Ampere equation (IV.1) cannot be used to advance E_T in time. Instead,

$$c^2\nabla^2 E_T = \frac{\partial J_T}{\partial t} \qquad (IV.3)$$

is used at time level n+1. This creates a time-centering problem. To preserve 2nd order accuracy in time, (IV.3) needs a time-advanced expression for $\partial J_T/\partial t$. To ensure stability, $\partial J/\partial t$ is expressed in terms of the advanced E, using moments accumulated from the particles:

$$\frac{\partial J}{\partial t} = -\nabla\cdot\rho\langle vv\rangle + (q\rho/m)E + (q\rho\langle v\rangle/mc)\times B \qquad (IV.4)$$

summed over species. This leads to an elliptic equation for the advanced fields of form

$$c^2\nabla^2 E_T - \omega_p^2(x)E_T = -\sum \nabla\cdot\rho\langle vv\rangle + (\sum q\rho\langle v\rangle/mc)\times B + \omega_p^2 E_L - \nabla F \qquad (IV.5)$$

at time level n+1. The divergence of this equation, together with $\nabla\cdot E_T = 0$, determines F. This elliptic equation provides instantaneous propagation of B and E_T, as is necessary for stability. Although this description uses moment equations, it seems possible to make a direct-method Darwin code.

After presenting the implicit algorithm, we make comparisons between the Darwin and the direct and moment implicit algorithms.

IV.B Implicit Electromagnetic Fields

Here we must select a time-differencing scheme for the fields, and find a method for solving the coupled field and particle equations. Desired features of the implicit differencing of the Maxwell equations include:

- At *long* wavelengths, accuracy in dispersion Re $\omega(k)$, and weak damping (e.g. Im $\omega(k)/ck = O(ck\Delta t)^3$; k is the wavevector).
- Stability (preferably damping) at *short* wavelengths $\cong 2\Delta x$ -stability despite $c\Delta t \gtrsim \Delta x$ (violation of the Courant condition for *explicit* differencing), and dissipation of inaccurately calculated short wavelengths.
- Compatible with implicit particles.
- Adaptable to general boundary conditions.
- Simplicity, and economy in storage.

- Optionally able to recover the centered 2nd order scheme now commonly used for the fields.

- Optionally able to recover the (nearly) centered Darwin scheme (Nielson and Lewis, 1976).

D_1 time differencing

For the time differencing of the fields, we adapt the D_1 implicit scheme developed for the particle equations of motion. For example, in the particle equations (I.9,I.10), drop the v×B term, replace x by E, v by c∇×B, and $\bar{a}$ by $-c^2\nabla\times\nabla\times\bar{E}$ to obtain the Maxwell equations in rationalized cgs units (Panofsky and Phillips, 1962; Jackson, 1962):

$$c\nabla\times B_{n+\frac{1}{2}} = J_{n+\frac{1}{2}} + \frac{E_{n+1} - E_n}{\Delta t} \qquad \text{(IV.6a)}$$

$$-c\nabla\times\bar{E}_n = \frac{B_{n+\frac{1}{2}} - B_{n-\frac{1}{2}}}{\Delta t} \qquad \text{(IV.6b)}$$

$$\text{where } \bar{E}_n = \tfrac{1}{2}[\bar{E}_{n-1} + E_{n+1}] \qquad \text{(IV.6c)}$$

is the result of a recursive low-pass filter with phase error $O(\Delta t^3)$. This phase error is an advance, not a lag as one gets if E_{n+1} is not used, so it provides stability when $ck\Delta t >> 1$; in this limit the fields are close to those in the Darwin approximation. Although equations (IV.6) are heuristically motivated, their desirable properties may be verified rigorously.

To advance the field values implicitly, eliminate E_{n+1} or $B_{n+\frac{1}{2}}$ from the coupled equations (IV.6) to obtain a single elliptic equation. Eliminating $B_{n+\frac{1}{2}}$ to form an equation for E_{n+1} yields

$$E_{n+1} + \tfrac{1}{2}c^2\Delta t^2\nabla\times\nabla\times E_{n+1} = E_n - J_{n+\frac{1}{2}}\Delta t + c\Delta t\nabla\times[B_{n-\frac{1}{2}} - \tfrac{1}{2}c\Delta t\nabla\times\bar{E}_{n-1}] \qquad \text{(IV.7)}$$

-or, eliminate E_{n+1} to form an equation for $B_{n+\frac{1}{2}}$:

$$B_{n+\frac{1}{2}} - \tfrac{1}{2}c^2\Delta t^2\nabla^2 B_{n+\frac{1}{2}} = B_{n-\frac{1}{2}} + \tfrac{1}{2}c\Delta t\nabla\times[J_{n+\frac{1}{2}} - \bar{E}_{n-1} - E_n] \qquad \text{(IV.8)}$$

In either case, the right-hand-side is composed of known fields. The left-hand-sides have well-behaved elliptic operators. In two dimensions (x,y), it is convenient to solve the z components of (IV.7) and (IV.8) for E_z and B_z respectively. This is two *scalar* uncoupled elliptic equations to solve. Then use (IV.6a) and (IV.6b) to find the other fields.

To form a B_n for use in the particle mover, we use e.g.

$$B_n = B_{n-\frac{1}{2}} - \tfrac{1}{2}\Delta t\ c\nabla\times E_n \qquad \text{(IV.9)}$$

We use E_n, rather than $\bar{E}_n$ as in (IV.6b), to simplify the linearized particle equation.

Eqs. (IV.6a-IV.6b) differ from the usual centered "leap-frog" scheme only in that the electric field in Faraday's law here is $\bar{E}_n$ instead of E_n. If we replace $\bar{E}_n$ in (IV.6b) with the linear combination $\alpha\bar{E}_n + (1-\alpha)E_n$, then with $\alpha=1$ we obtain the D_1 scheme above, and the leap-frog scheme with $\alpha=0$. For intermediate values the upper bound on Δt increases as $\alpha \to 1$. In problems where most cells are large and the undamped leap-frog scheme is preferred, but some cells are much smaller (e.g. near a boundary, or for $r\to 0$ in cylindrical or spherical coordinates), one might use $\alpha=0$ for the large cells and increase α to maintain stability where cells are smaller. B. Godfrey (private communication) observes that electromagnetic wave dispersion is improved by operating close to the stability boundary.

IV.C The Direct Method for Implicit Particles and Fields

As in Section II.A.4 for the electrostatic case, the source terms in Maxwell's equations (IV.6) are the densities $\{\rho^{(0)}_{n+1}, J^{(0)}_{n+\frac{1}{2}}\}$ and $\{\delta\rho, \delta J\}$ corresponding to the extrapolations $\{x^{(0)}_{n+1}, v^{(0)}_{n+\frac{1}{2}}\}$, plus the increments $\{\delta x, \delta v\}$ which depend on E_{n+1}.

Evaluation of the extrapolated densities.

The extrapolated current and charge densities $\{\rho^{(0)}_{n+1}, J^{(0)}_{n+\frac{1}{2}}\}$ are evaluated as in explicit codes, such as ZOHAR (Langdon and Lasinski, 1976) and the Los Alamos WAVE code, from $x^{(0)}_{n+1}$, $v^{(0)}_{n+\frac{1}{2}}$ and x_n. At the grid point located at X_j,

$$\rho^{(0)}_{n+1} = \sum qS(X_j - x^{(0)}_{n+1}) \qquad \text{(IV.10)}$$

$$\text{and } J^{(0)}_{n+\frac{1}{2}} = \sum qv^{(0)}_{n+\frac{1}{2}}\, S(X_j - \tfrac{1}{2}[x_n + x^{(0)}_{n+1}]) \qquad \text{(IV.11a)}$$

$$\text{or} \qquad = \sum qv^{(0)}_{n+\frac{1}{2}}\, \tfrac{1}{2}[S(X_j - x_n) + S(X_j - x^{(0)}_{n+1})] \qquad \text{(IV.11b)}$$

Neither expression for $J^{(0)}_{n+\frac{1}{2}}$ is quite consistent with $\rho^{(0)}_{n+1}$ and the continuity equation, in that

$$\nabla\cdot J^{(0)}_{n+\frac{1}{2}} + (\rho^{(0)}_{n+1} - \rho_n)/\Delta t \neq 0 \qquad \text{(IV.12)}$$

While it is possible to construct a J which does conserve charge, it has been preferable in most explicit codes to use the above J and then to apply a correction to the longitudinal component of J or of E_{n+1} (Boris, 1970; Langdon and Lasinski, 1976). Here, we replace $J^{(0)}_{n+\frac{1}{2}}$ with

$$J'_{n+\frac{1}{2}} = J^{(0)}_{n+\frac{1}{2}} + (\nabla\psi)/\Delta t, \qquad \text{(IV.13a)}$$

where $$-\nabla^2\psi = \rho^{(0)}_{n+1} + \nabla\cdot[\Delta t J^{(0)}_{n+\frac{1}{2}} - E_n]. \qquad \text{(IV.13b)}$$

Note that the source term for ψ would vanish if $J^{(0)}_{n+\frac{1}{2}}$ were consistent with $\rho^{(0)}_{n+1}$ and ρ_n. Derivation of (IV.13b), and an alternate correction to E_{n+1}, are discussed below.

Evaluation of the increments due to future fields.

The care with which we express the increments $\{\delta\rho,\delta J\}$ is a compromise between complexity and strong convergence. If necessary, they may be evaluated rigorously as derivatives of equations (IV.10) and (IV.11) ("strict differencing", Section II.A.2, and Langdon *et al*, 1983, section 4), or as simplified difference representations (Section II.A.2) of

$$\delta\rho = -\nabla\cdot[\rho\delta x], \qquad \text{(IV.14)}$$

$$\delta J = \rho\delta v - \tfrac{1}{2}\nabla \times (J \times \delta x) \qquad \text{(IV.15)}$$

for each species. This form for δJ trivially conserves charge: $\delta\rho + \Delta t\nabla\cdot\delta J = 0$. This property can easily be preserved in the spatial differencing of δJ.

The terms in Eq. (IV.15) have both analytic and pictorial justifications; see Fig. 5. A heuristic derivation of δJ uses an analogy to magnetization current. The magnetic moment of the current loop in the last diagram is

$$(I/2c)\int x \times dx = (q/2c\Delta t)\delta x \times (v^{(0)}_{n+\frac{1}{2}}\Delta t).$$

The current due to a density n(x) of these loops is

$$\delta J = c\nabla\times M = c\nabla\times[n(q/2c\Delta t)\ \delta x \times v^{(0)}_{n+\frac{1}{2}}\Delta t] = \tfrac{1}{2}\nabla\times[\delta x \times \rho v^{(0)}_{n+\frac{1}{2}}]$$

which leads to the last term in (IV.15). A related term arises in linearized particle codes (Cohen *et al*, 1980).

A careful examination of the locations at which $\mathbf{E}$ and $\delta\mathbf{J}$ are evaluated in Eq. (IV.15) shows a $O(kv\Delta t)^2$ error. Because its phase is neutral, this error is expected to be innocuous.

Construction of the Implicit Field Equation

We now have everything needed to write an equation for $\mathbf{E}_{n+1}$. On substituting our expressions for $\mathbf{J}^{(0)}_{n+\frac{1}{2}}$ and $\delta\mathbf{J}$ into the field equations (IV.6-IV.7), we have

$$c\nabla \times \left[\mathbf{B}_{n+\frac{1}{2}} + (\mathbf{J}^{(0)}_{n+\frac{1}{2}} \times \delta\mathbf{x})/2c \right] = \mathbf{J}'_{n+\frac{1}{2}} + \rho^{(0)}_{n+1}\delta\mathbf{v} + \frac{\mathbf{E}_{n+1} - \mathbf{E}_n}{\Delta t} \qquad \text{(IV.16a)}$$

$$-\tfrac{1}{2}\, c\nabla \times \left[\bar{\mathbf{E}}_{n-1} + \mathbf{E}_{n+1}\right] = \frac{\mathbf{B}_{n+\frac{1}{2}} - \mathbf{B}_{n-\frac{1}{2}}}{\Delta t} \qquad \text{(IV.16b)}$$

With (II.18), the implicit terms $\rho\delta\mathbf{v}$ and $\mathbf{J}\times\delta\mathbf{x}$ are seen to be

$$\rho^{(0)}_{n+1}\delta\mathbf{v} = \left[\sum_s \frac{\rho_s q_s \Delta t}{2m_s}\, \tfrac{1}{2}(\mathbf{I}+\mathbf{R}_s)\right]\cdot\mathbf{E}_{n+1} \quad = \chi\cdot\mathbf{E}_{n+1}/\Delta t \qquad \text{(IV.17a)}$$

$$\mathbf{J}^{(0)}_{n+\frac{1}{2}} \times \delta\mathbf{x} = \left[\sum_s \frac{\mathbf{J}_s q_s \Delta t^2}{2m_s} \times \tfrac{1}{2}(\mathbf{I}+\mathbf{R}_s)\right]\cdot\mathbf{E}_{n+1} = c\xi\cdot\mathbf{E}_{n+1} \qquad \text{(IV.17b)}$$

The [...] are sums over *species*, not each particle. If only the electrons are implicit, only they appear in (IV.17). In this case, the terms [...] require only a knowledge of the electrons' ρ and $\mathbf{J}$ (in addition to the *net* ρ and $\mathbf{J}$ used on the right side of (IV.16a)). In general, it is sufficient to accumulate $\rho^{(0)}_{n+1,s}$ and $\mathbf{J}^{(0)}_{n+\frac{1}{2},s}$ separately from species with differing q/m. This requires more storage, but *no more computation* than for an explicit code.

Spatial differencing, follows in spirit the "simplified differencing" of Section II.A.

Due to the correction (EA.18), the divergence of the Ampere-Maxwell equation (IV.16a) recovers *exactly* our *electrostatic* implicit field equation, (II.21) with $\mathbf{E}^{(0)}_{n+1} = 0$ and $\mathbf{E}_{n+1} = -\nabla\delta\phi_{n+1}$.

Equations (IV.16) and (IV.17) are the simplest yet proposed for implicit field prediction, both in themselves and in what one must accumulate from the particles.

Longitudinal Field Correction

As mentioned above, the solution of (IV.16a) would fail slightly to satisfy the longitudinal equation corresponding to (II.21),

$$\nabla\cdot(1+\chi)\cdot\mathbf{E}_{n+1} = \rho^{(0)}_{n+1} \tag{IV.18}$$

if $\mathbf{J}'_{n+\frac{1}{2}}$ were not used in place of $\mathbf{J}^{(0)}_{n+\frac{1}{2}}$. Equation (IV.13b) for the correction is derived by substituting (IV.13a) and (IV.17a) into (IV.16a), taking the divergence, and comparing to (IV.18).

Alternatively, one could apply a longitudinal correction to the solution of (IV.16a) with $\mathbf{J}^{(0)}_{n+\frac{1}{2}}$ used for $\mathbf{J}'_{n+\frac{1}{2}}$. That is, rewrite (IV.16a) with (IV.17a) as

$$c\Delta t\nabla \times [..] = \mathbf{J}^{(0)}_{n+\frac{1}{2}}\Delta t + \chi\cdot\mathbf{E}' + (\mathbf{E}' - \mathbf{E}_n) \tag{IV.19}$$

and solve for $\mathbf{E}'$, from which $\mathbf{E}_{n+1} = \mathbf{E}' - \nabla\psi$. Comparing the divergence of (IV.19) to (IV.18) gives

$$-\nabla\cdot(1+\chi)\cdot\nabla\psi = \rho^{(0)}_{n+1} - \nabla\cdot(1+\chi)\cdot\mathbf{E}' \tag{IV.20}$$

With $\chi \ll 1$, this step corresponds to Boris' correction to $\nabla\cdot\mathbf{E}_{n+1}$, and has the identical result to the correction to J (Langdon and Lasinski, 1976). Here the transverse part of $\mathbf{E}_{n+1}$ differs between the two methods; the correction (IV.20) corresponds nearly to using $(1+\chi)\cdot\nabla\psi$ instead of $\nabla\psi$ in (IV.13a).

IV.D Comparison of Darwin and Implicit Codes

The need for time-advanced currents, and expressing their dependence on the advanced fields, are central to both Darwin and implicit codes. Indeed, the direct-implicit codes were conceived with Darwin codes in mind. The similarity to moment-implicit methods, in which (IV.4) is a key equation, is obvious. In the Darwin code of (Nielson and Lewis, 1976), although the particle integration remains explicit, they paid most of the price of being fully implicit.

With explicit time differencing in a Darwin code, the time step is still limited by the electron plasma period and Alfven wave periods. The field solution in Darwin codes is complicated by the separation of longitudinal and transverse components of E. Implicit approaches may subsume the Darwin model in many applications. On the other hand, when electromagnetic wave propagation is not required, nonphysical dissipation due to implicit differencing of the fields could make the Darwin model more accurate.

V. CONCLUDING REMARKS

In this Chapter we apply the "direct" method to derive implicit PIC algorithms that are simpler, and less restrictive in some respects, than the "moment" algorithms published to date. A strict application of the direct viewpoint provides tools for analysis of the convergence and stability of both direct and moment algorithms, and shows how to enforce properties such as momentum conservation. Analytic insights and experience in applications gained with both methods have begun to advance the development of each. As moment and direct codes are borrowing features from each other, the distinction becomes more that of viewpoint in deriving algorithms and less in the resulting codes themselves.

We have not discussed boundary conditions. In implicit codes, particle boundary conditions can be complex. Particle deletion or emission at a surface depends on $\mathbf{E}_{n+1}$; therefore the particle boundary conditions enter into the implicit field equations. For electromagnetic fields it appears that methods used in explicit codes can be adapted. At Palaiseau for example, Adam and Gourdin have adapted the outgoing-wave boundary conditions of Lindman (1975) by using implicit differencing of his boundary wave equations.

Many generalizations are possible. To include relativity, one would linearize the relativistic particle equation-of-motion (Langdon and Lasinski, 1976; Boris, 1970). In practice, this adds complexity because the susceptibility χ becomes velocity-dependent. Electron-ion collisions ($\nu \lesssim \Delta t^{-1}$) may be described as an addition to the rotation R in the equation-of-motion. If a component of the plasma is modeled by fluid equations then those equations are linearized to find $\{\delta\rho, \delta J\}$ (Denavit, 1984). Combining fluid and particle descriptions is difficult, but not more so in the direct method than in the moment method.

ACKNOWLEDGMENTS

This work is an outgrowth of our stimulating and productive collaborations with B. I. Cohen, A. Friedman, D. W. Hewett, T. Kamimura, J.-N. LeBoeuf and T. Tajima. It is a pleasure to acknowledge valuable conversations with J. C. Adam, J. U. Brackbill, J. Denavit, D. Forslund, B. Godfrey, A. Gourdin Heron, R. J. Mason, and D. Nielson. This work was performed under the auspices of the U. S. Department of Energy by the Lawrence Livermore Laboratory under Contract No. W-7405-Eng-48, and the Institute for Fusion Studies under Contract No. DE-FG05-80ET-53088.

REFERENCES

J. C. Adam, A. Gourdin Serveniere, A. B. Langdon, "Electron Sub-Cycling in Particle Simulation of Plasmas", *J. Comp. Phys.* 47 (1982), 229.

D. C. Barnes and T. Kamimura, "LOMEGA: A Low Frequency, Field Implicit Method for Plasma Simulation", Institute of Plasma Physics, IPPJ-570, Nagoya University, April 1982.

D. C. Barnes, T. Kamimura, J.-N. Leboeuf, and T. Tajima, paper 2A4, Proceedings of the Tenth Conference on Numerical Simulation of Plasmas, San Diego, CA, Jan. 4-6, 1983a.

D. C. Barnes, T. Kamimura, J.-N. LeBoeuf and T. Tajima, "Implicit Particle Simulation of Magnetized Plasmas", *J. Comp. Phys.* 52, 480 (1983b).

C. K. Birdsall and D. Fuss, *J. Comput. Phys.* 3, 494 (1969).

C. K. Birdsall and A. B. Langdon, "Plasma Physics Via Computer Simulation", McGraw-Hill, New York, 1984, Chapter 12.

J. P. Boris and K. V. Roberts, *J. Comput. Phys.* 4, 552 (1969).

J. P. Boris, "Relativistic Plasma Simulation -Optimization of a Hybrid Code", *Proceedings of the Fourth Conference on Numerical Simulation of Plasmas*, Nov. 1970.

J. U. Brackbill and D. W. Forslund, "An Implicit Method for Electromagnetic Plasma Simulation in Two Dimensions", *J. Comp. Phys.* 46 (1982), 271.

J. U. Brackbill and D. W. Forslund, "Simulation of low frequency, electromagnetic phenomena in plasmas", a chapter in this volume.

A. Brandt, *Math. Comp.* 31, 333 (1977).

O. Buneman, *J. Comp. Phys.* 1 (1967), 517.

P. Burger, D. A. Dunn, and A. S. Halstead, *Phys. Fluids* 8, 2263 (1965).

J. Busnardo-Neto, P. L. Pritchett, A. T. Lin, and J. M. Dawson, *J. Comput. Phys.* 23, 300 (1977).

B. I. Cohen, S. P. Auerbach and J. A. Byers, "Some Conservation Properties of Linearized Particle Codes", *Phys. Fluids* 23 (1980), 2529.

B. I. Cohen, R. P. Freis and V. Thomas, "Orbit-Averaged Implicit Particle Codes", *J. Comp. Phys.* 45 (1982a), 345.

B. I. Cohen, A. B. Langdon and A. Friedman, "Implicit Time Integration for Plasma Simulation", *J. Comp. Phys.* 46 (1982b), 15.

B. I. Cohen, A. B. Langdon and A. Friedman, "Smoothing and Spatial Grid Effects in Direct Implicit Particle Simulation", UCRL-88363, LLNL, September 1983, submitted to *J. Comput. Phys.* Also, paper 1C15, *Proceedings of the Tenth Conference on Numerical Simulation of Plasmas*", San Diego, CA, Jan. 4-6, 1983.

B. Cohen, "Orbit averaging and sub-cycling in particle simulation of plasma", UCRL-89668, a chapter in this volume.

P. Concus and G. H. Golub, *SIAM J. Numer. Anal.* 10, 1103 (1973).

J. Denavit, "Time Filtering Particle Simulations with $\omega_{pe}\Delta t>>1$", *J. Comp. Phys.* 42 (1981), 337.

J. D. Denavit, "One-Dimensional Time-Implicit Hybrid Simulation", to be published, and "One-Dimensional Time-Implicit Hybrid Simulations", paper 1B15, *Proceedings of the Tenth Conference on Numerical Simulation of Plasmas*", San Diego, CA, Jan. 4-6, 1983.

S. Doss and K. Miller, *SIAM J. Numer. Anal.* 16, 837 (1979).

D. H. E. Dubin, J. A. Krommes, C. Oberman, W. W. Lee, "Nonlinear Gyrokinetic Equations", *Phys. Fluids* 26, 3524 (1983).

D. W. Forslund and J. U. Brackbill, "Magnetic Field Induced Surface Transport on Laser Irradiated Foils", *Phys. Rev. Lett.* 48 (1982), 1614.

A. Friedman, A. B. Langdon and B. I. Cohen, "A Direct Method for Implicit Particle-in-Cell Simulation", *Comments on Plasma Physics and Controlled Fusion* 6 (1981), 225.

A. Friedman, A. B. Langdon and B. I. Cohen, *Laser Program Annual Report-1982*, Lawrence Livermore National Laboratory, Livermore, CA, UCRL-80021-82 (1983), p. 3-56.

D. W. Hewett, "A Global Method of Solving the Electron-Field Equations in a Zero-Inertia-Electron-Hybrid Plasma Simulation Code", *J. Comput. Phys.* 38, 378 (1980).

R. W. Hockney, *J. Assoc. Comput. Mach.* 12, 95 (1965).

J. D. Jackson, *Classical Electrodynamics* (Wiley, New York, 1962), p. 616 ff.

A. N. Kaufman and P. S. Rostler, "The Darwin Model as a Tool for Electromagnetic Plasma Simulation", *Phys. Fluids* 14 (1971), 446.

D. S. Kershaw, "The Incomplete Cholesky-Conjugate Gradient Method for the Iterative Solution of Systems of Linear Equations", *J. Comput. Phys.* 26, 43 (1978).

D. S. Kershaw, "On the Problem of Unstable Pivots in the Incomplete LU-Conjugate Gradient Method", *J. Comput. Phys.* 38, 114 (1980).

A. B. Langdon, "Nonphysical Modifications to Oscillations, Fluctuations and Collisions due to Space-Time Differencing", *Proceedings of the Fourth Conference on Numerical Simulation of Plasmas*, Nov. 1970.

A. B. Langdon, *J. Comp. Phys.* 6 (1970), 247.

A. B. Langdon and C. K. Birdsall, *Phys. Fluids* 13 (1970), 2115.

A. B. Langdon, *J. Comp. Phys.* 12 (1973), 247.

A. B. Langdon and B. F. Lasinski, "Electromagnetic and Relativistic Plasma Simulation Models", in "Methods in Computational Physics", (B. Alder, S. Fernbach, and M, Rotenberg, Eds, Volume Ed. J. Killeen), p. 327, Academic Press, New York, 1976.

A. B. Langdon, *J. Comp. Phys.* 30 (1979), 202.

A. B. Langdon, *Phys. Fluids* 22 (1979), 163.

A. B. Langdon, "Electromagnetic Direct Implicit PIC Simulation", UCRL-88979, March 1983; and *Laser Program Annual Report-1982*, Lawrence Livermore National Laboratory, Livermore, CA, UCRL-80021-82 (1983), p. 3-53.

A. B. Langdon, B. I. Cohen and A. Friedman, "Direct Implicit Large-Timestep Particle Simulation of Plasma", *J. Comp. Phys.* 51 (1983), 107.

A. B. Langdon, D. W. Hewett and A. Friedman, *Laser Program Annual Report-1983*, Lawrence Livermore National Laboratory, Livermore, CA, UCRL-80021-83 (1984).

J. N. Leboeuf, T. Tajima, A. Y. Aydemir, D. C. Barnes, and T. Kamimura, *Bull. Am. Phys. Soc.*, 27, 1035 (1982).

W. W. Lee, *Phys. Fluids*, 26, 556 (1983).

E. L. Lindman, *J. Comput. Phys.* 18, 66 (1975).

R. J. Mason, "Implicit Moment Particle Simulation of Plasmas", *J. Comp. Phys.* 41 (1981), 233.

R. J. Mason, "Apparent and Real Thermal Inhibition in Laser-Produced Plasmas", *Phys. Rev. Lett.* 47 (1981), 652.

R. J. Mason, "Hybrid and collisional implicit plasma simulation models", a chapter in this volume.

R. L. Morse and C. W. Nielson, *Phys. Fluids* 12, 2418 (1969).

R. L. Morse, in *Methods in Computational Physics*, edited by B. Alder, S. Fernbach, and M. Rotenberg (Academic, New York, 1970), Vol. 9, p. 213.

C. W. Nielson and H. R. Lewis, "Particle Code Models in the Nonradiative Limit", in "Methods in Computational Physics", (B. Alder, S. Fernbach, and M. Rotenberg, Eds, Vol. Ed. J. Killeen), p. 367, Academic Press, N.Y., 1976.

T. G. Northrup, *Annals of Phys.* 15, 19 (1961).

J. H. Orens, J. P. Boris, and I. Haber, in *Proceedings of the Fourth Conference on the Numerical Simulation of Plasmas*, edited by J. P. Boris and R. Shanny (U. S. Government Printing Office, Washington, D. C.), p. 526.

W. K. H. Panofsky and M. Phillips, *Classical Electricity and Magnetism* (Addison-Wesley, Reading, Massachusetts, 1962), p. 461.

M. Petravic and G. Kuo-Petravic, "An ILUCG Algorithm Which Minimizes in the Euclidean Norm", *J. Comput. Phys.* 32, 263 (1979).

H. Sakagami, K. Nishihara and D. Colombant, "Stability of Time-Filtering Particle Code Simulation", Institute of Laser Engineering report ILE8117P, August 10, 1981.

T. Tajima and J. N. Leboeuf, *Bull. Am. Phys. Soc.*, 26, 986 (1981).

S. P. Yu, G. P. Kooyers, and O. Buneman, *J. Appl. Phys.* 36, 2550 (1965).

FIGURES

1. Total energy normalized to its t=0 value, as a function of time.

2. Fluctuation spectrum for thermal plasma. Normalized electrostatic field energy as a function of wavenumber is shown. Upper curve is theory including electron Landau damping; lower curve is theory neglecting electron Landau damping; points are simulation results.

3. Electrostatic field energy (normalized) as a function of time for unstable gravitational interchange.

4. Snapshots of finite size ion density contours are shown, along with point plots of ion positions for three times near saturation of gravitational interchange. a) $\omega_{pe}t = 3\times10^5$, b) $\omega_{pe}t = 4\times10^5$, c) $\omega_{pe}t = 5\times10^5$.

5. Geometric interpretation of the terms in $J_{n+1} = J^{(0)}_{n+\frac{1}{2}} + \delta J$: While $J_{n+\frac{1}{2}}$ corresponds to moving the particle *directly* from x_n to x_{n+1}, it can be regarded as the sum of 3 motions: (1) motion from x_n to $x^{(0)}_{n+1}$, giving $J^{(0)}_{n+\frac{1}{2}}$, (2) then motion from $x^{(0)}_{n+1}$ to x_{n+1}, giving $\rho\delta v$ plus (3) a circulation term $-\frac{1}{2}\nabla\times(J\times\delta x)$ to cancel the effect of the "detour" to $x^{(0)}_{n+1}$. This is not needed to get ρ_{n+1} but does affect B and E_T.

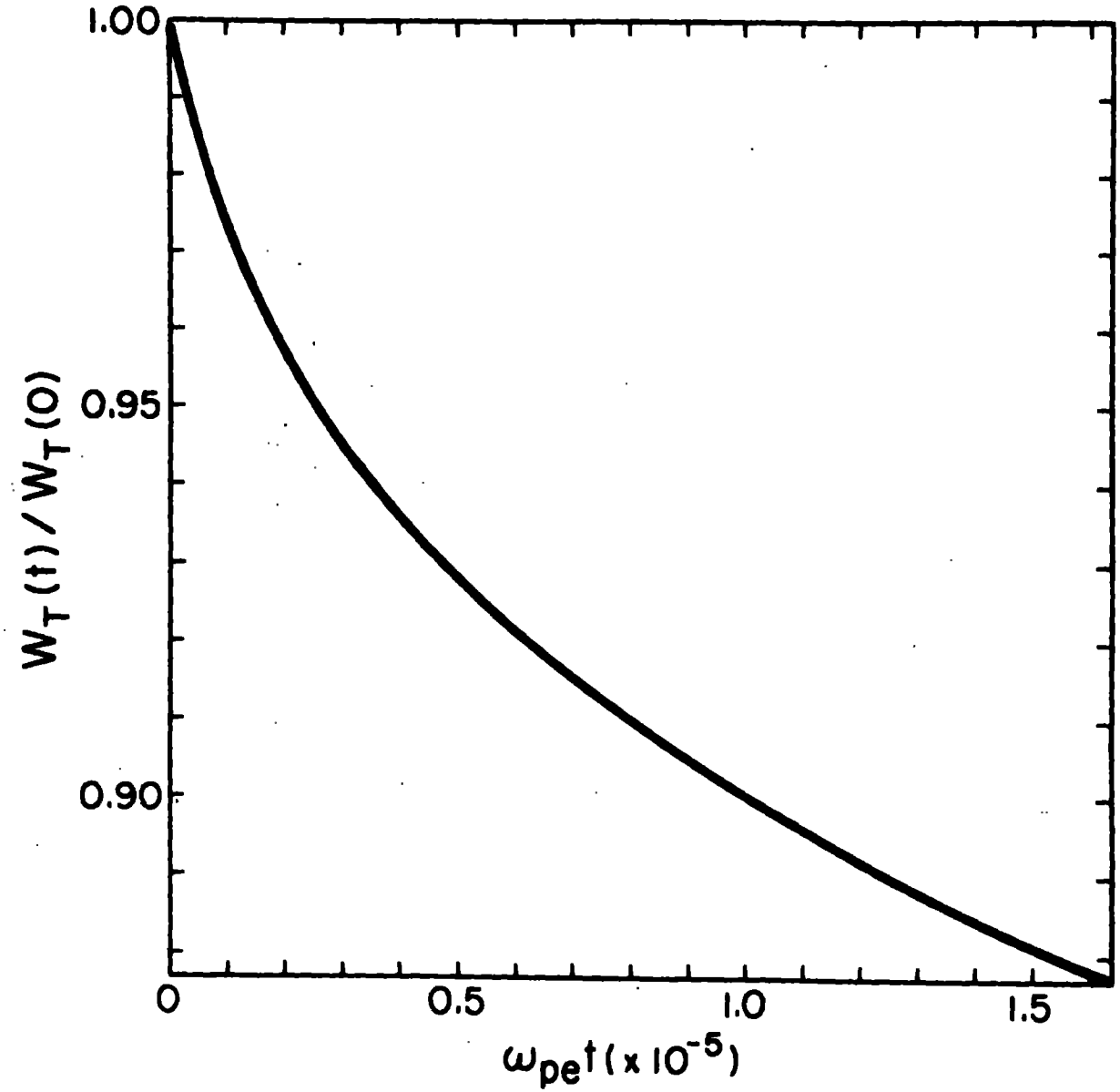
1.00
0.95
0.90
$W_T(t) / W_T(0)$
0
0.5
1.0
1.5
$\omega_{pe} t\ (\times 10^{-5})$

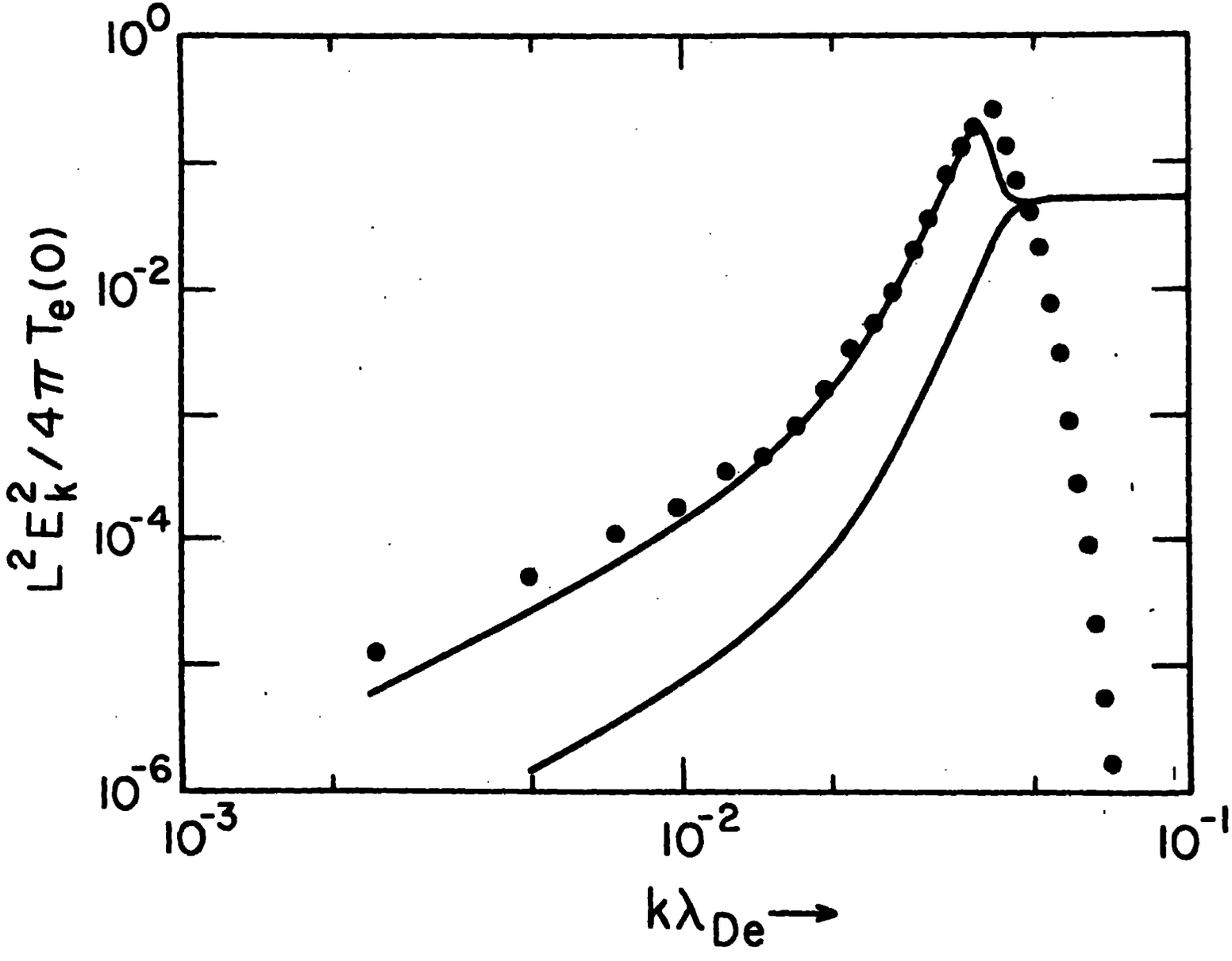
10^0
10^{-2}
10^{-4}
10^{-6}
$L^2E_k^2/4\pi T_e(0)$
10^{-3}
10^{-2}
10^{-1}
$k\lambda_{De}\rightarrow$

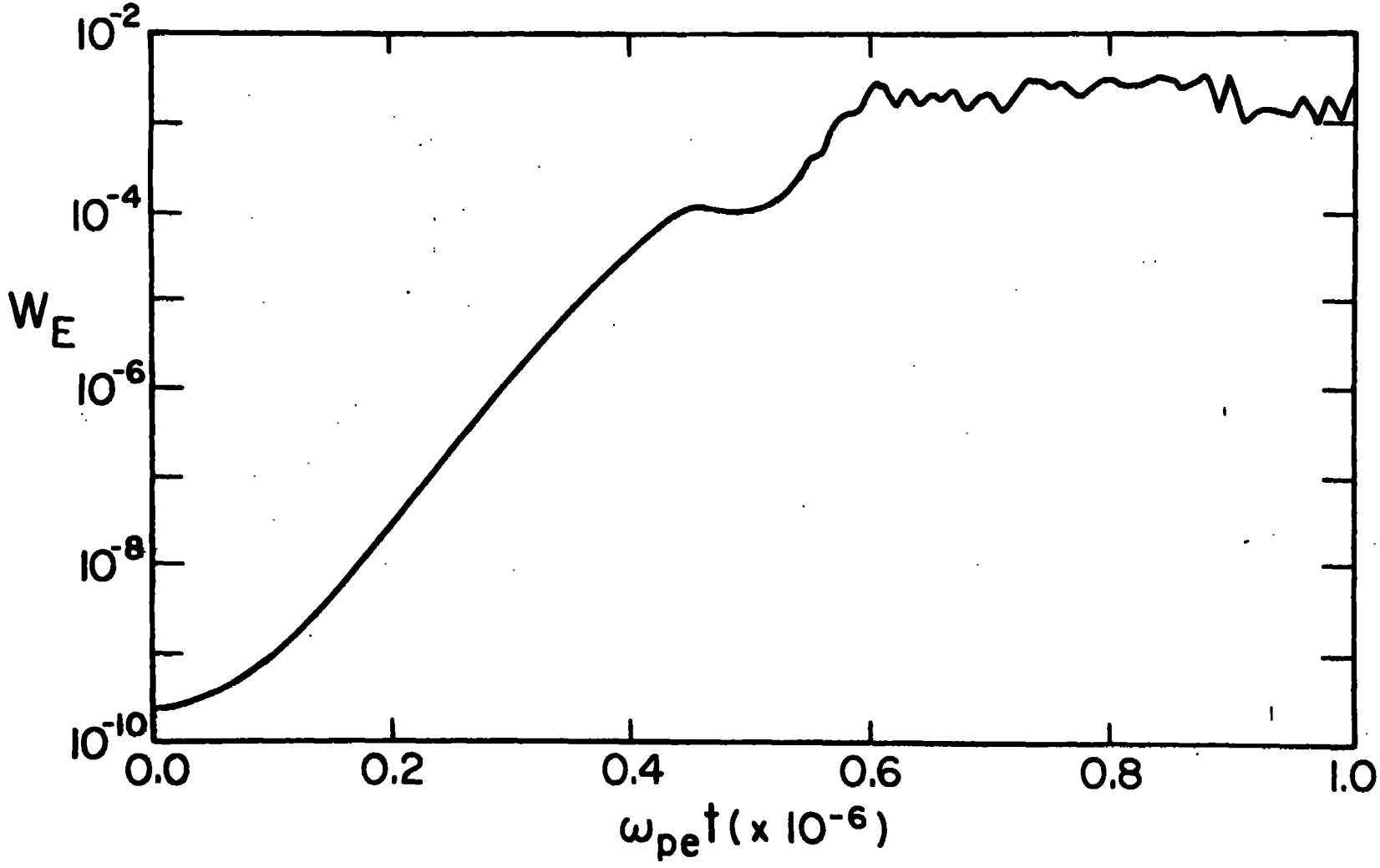
10^{-2}
10^{-4}
W_E
10^{-6}
10^{-8}
10^{-10}
0.0
0.2
0.4
0.6
0.8
1.0
$\omega_{pe}t\,(\times 10^{-6})$

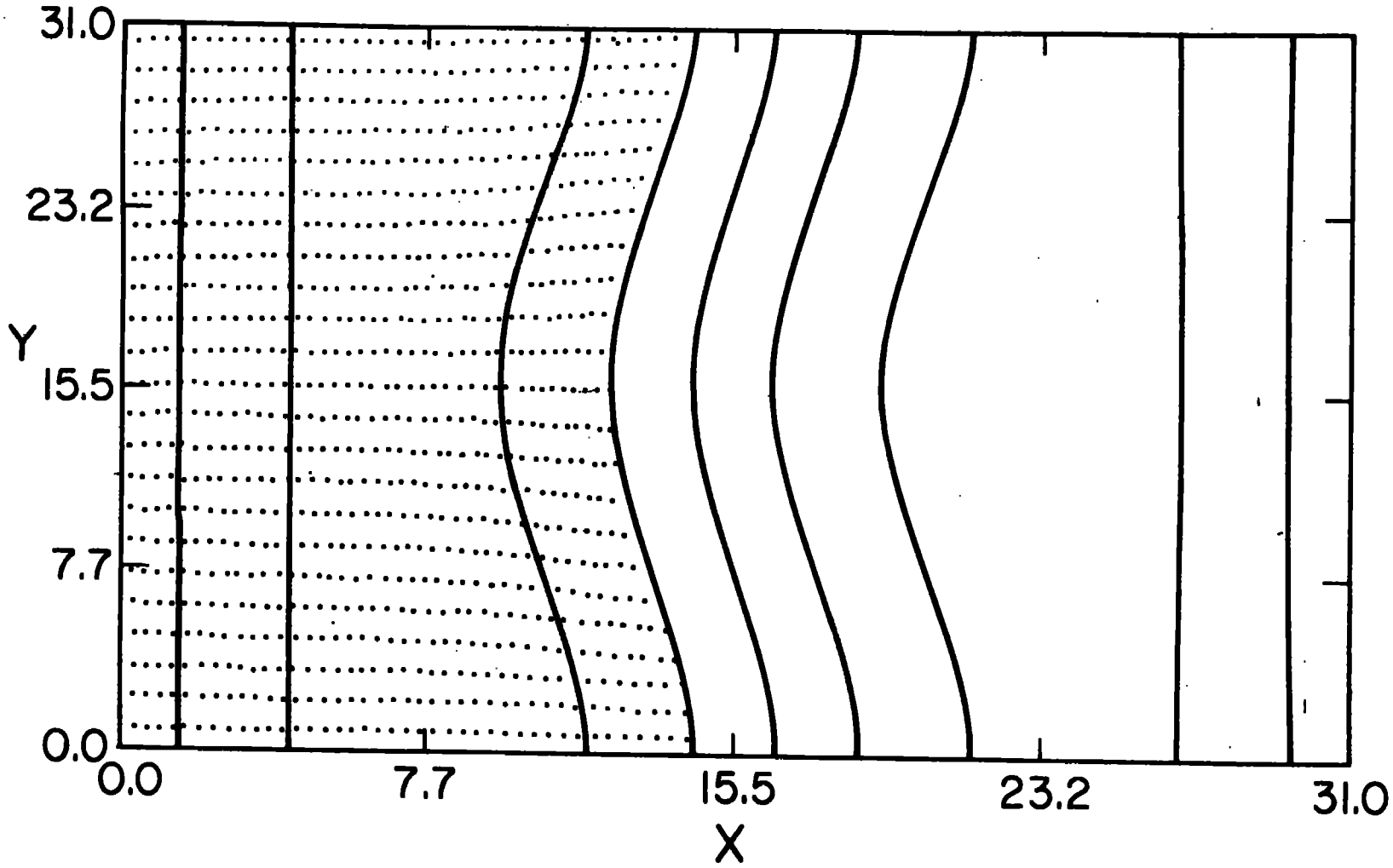

4a

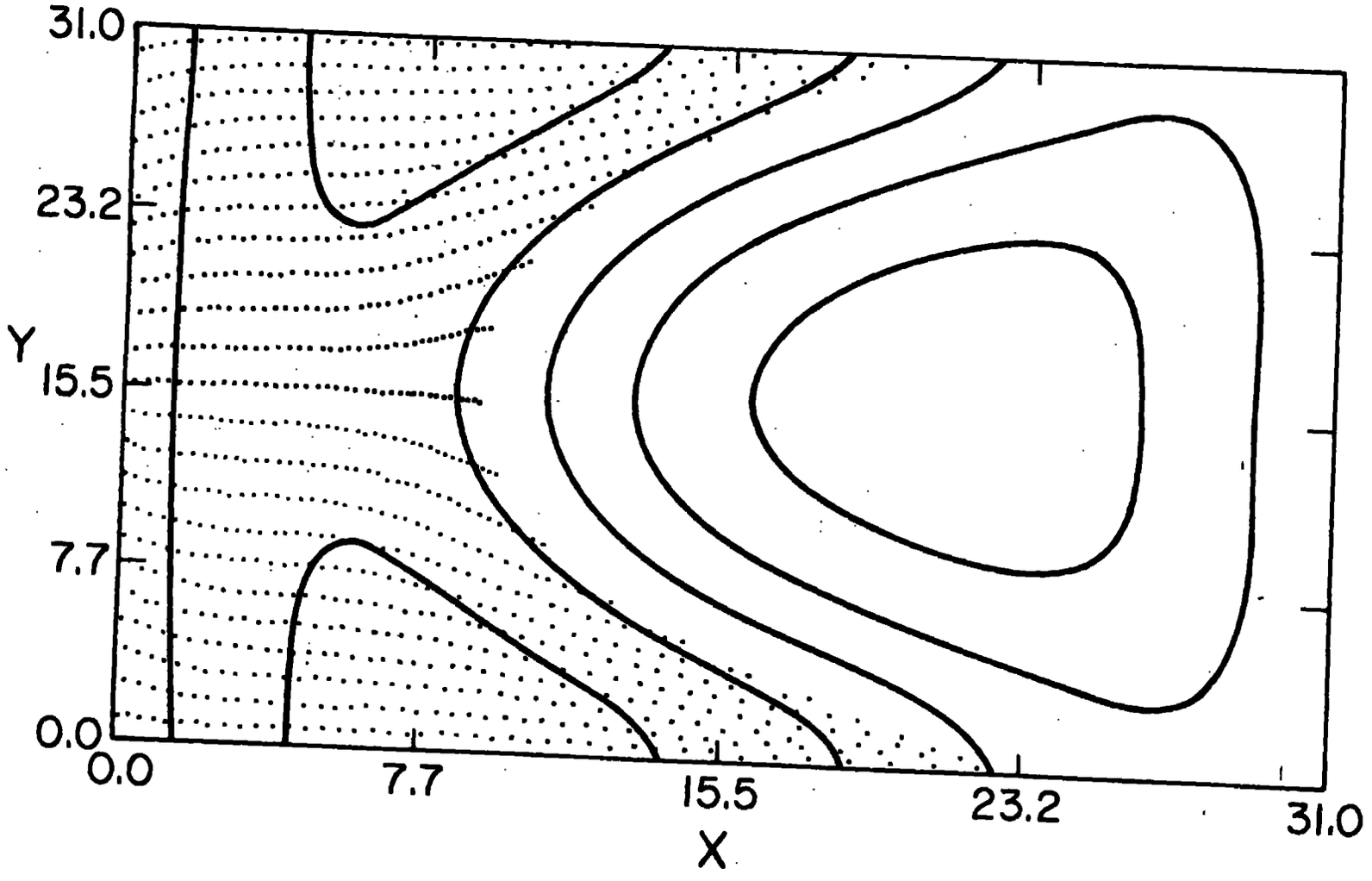
31.0
23.2
15.5
7.7
0.0
Y
0.0
7.7
15.5
23.2
31.0
X

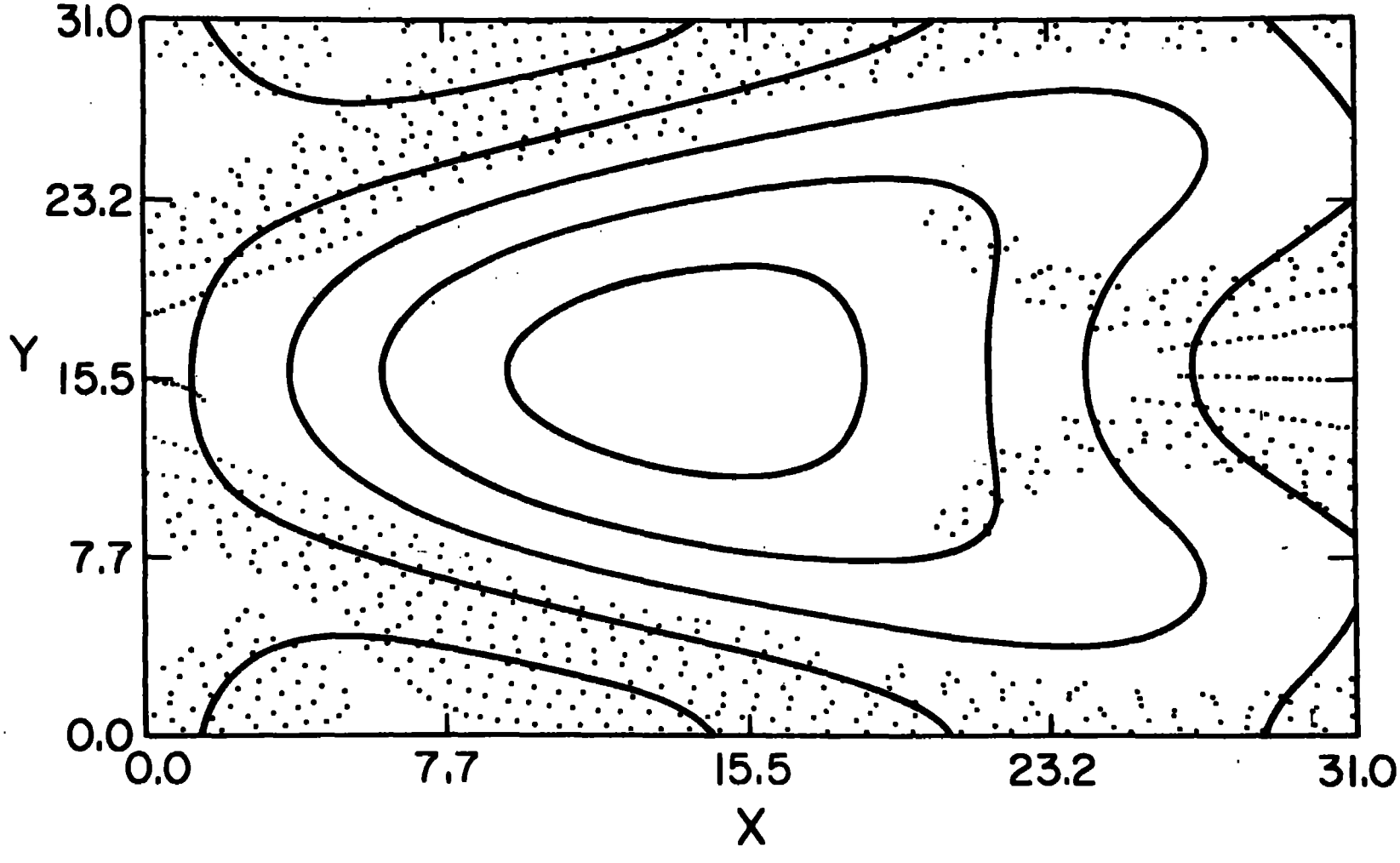

4c

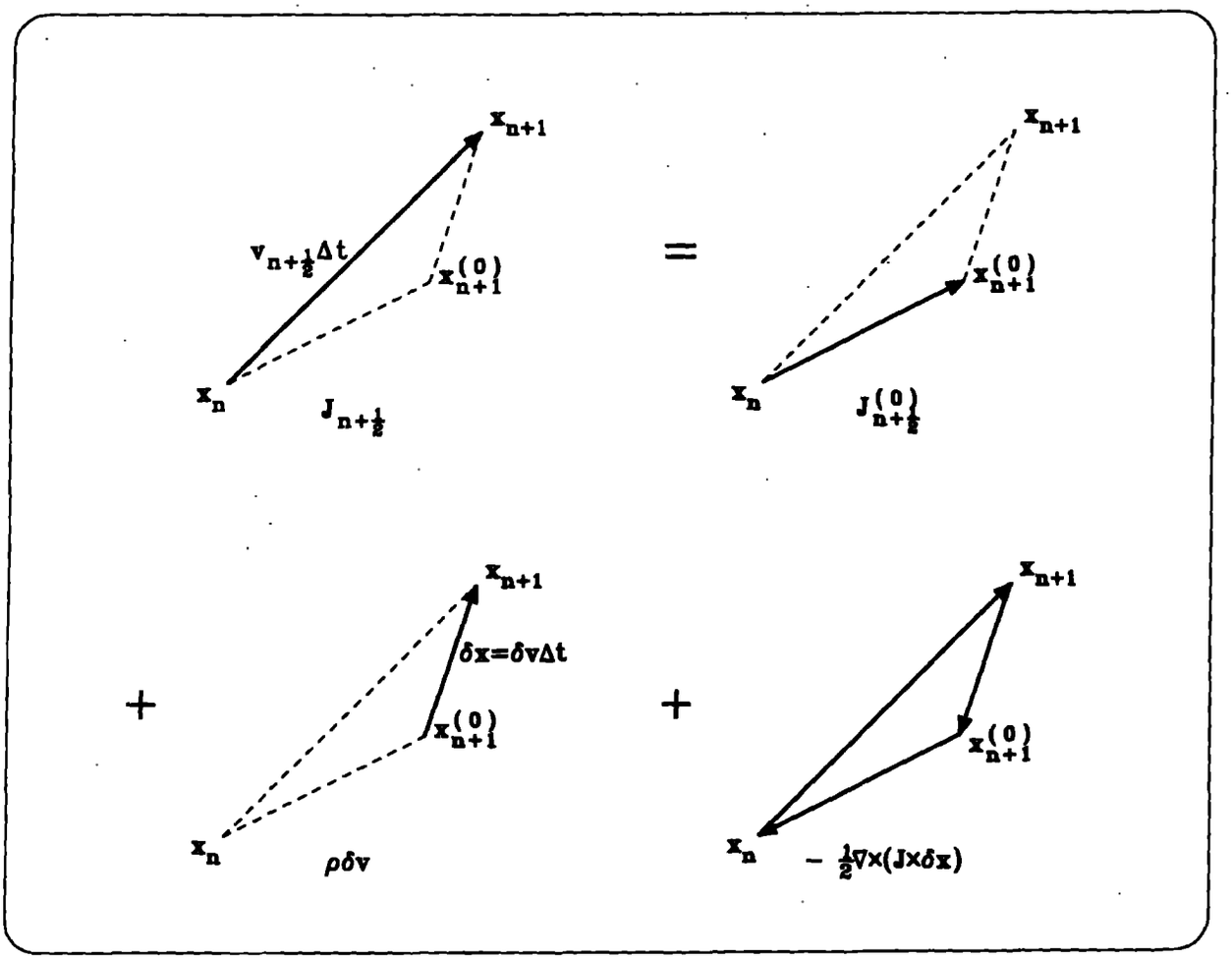

Figure 5 Langdon and Barnes